

Highly Ionized High Velocity Clouds: Intergalactic Gas in the Local Group or Distant Gas in the Galactic Halo?¹

Kenneth R. Sembach

Department of Physics & Astronomy, The Johns Hopkins University, Baltimore, MD 21218

sembach@sundoggie.pha.jhu.edu

Blair D. Savage

Department Astronomy, The University of Wisconsin, Madison, WI 53706

savage@astro.wisc.edu

Limin Lu²

Department Astronomy, 105-24, California Institute of Technology 91125

ll@troyte.caltech.edu

Edward M. Murphy

Department of Physics & Astronomy, The Johns Hopkins University, Baltimore, MD 21218

emurphy@pha.jhu.edu

Received _____; accepted _____

¹Based on observations obtained with the NASA/ESA Hubble Space Telescope, obtained at the Space Telescope Science Institute, which is operated by the Association of Universities for Research in Astronomy, Inc. under NASA contract NAS5-26555.

²Hubble Fellow

ABSTRACT

In the course of our studies of the gaseous halo surrounding the Milky Way, we have recently identified several high velocity ($V_{\text{LSR}} < -100 \text{ km s}^{-1}$) clouds in the directions of Mrk 509 and PKS 2155-304 that have unusual ionization properties. The clouds exhibit strong C IV absorption with little or no detectable low ion (C II, Si II) absorption or H I 21 cm emission down to very sensitive levels. As the closest known analog to the outer diffuse halos of damped Ly α absorbers and the low H I column density metal line absorption systems seen in the spectra of high redshift quasars, these “C IV-HVCs” present unique opportunities for relating the conditions within the Milky Way halo and nearby intergalactic gas to the properties of galactic halos at higher redshift.

In this paper we present new Goddard High Resolution Spectrograph intermediate-resolution measurements of the absorption lines within these C IV-HVCs and study the ionization properties of the gas in detail. The present data represent the most complete set of measurements available for studying the ionization conditions within high velocity clouds. The C IV-HVCs have ionization properties consistent with photoionization by extragalactic background radiation, though some contribution by collisional ionization within a hot plasma cannot be ruled out. The clouds are probably low density ($n_H \sim 10^{-4} \text{ cm}^{-3}$), large (greater than several kiloparsecs), and mostly ionized ($n_{\text{HI}}/n_H \sim 10^{-3}$) regions located well beyond the neutral gas layer of the Galaxy. The presence of weak H I-HVCs detected through their 21 cm emission near both sight lines indicates that the C IV-HVCs trace the extended, ionized, low density regions of the H I-HVCs. Several lines of evidence, including very low thermal pressures ($P/k \sim 2 \text{ cm}^{-3} \text{ K}$), favor a location for the C IV-HVCs in the Local Group or very distant Galactic halo. Group. If the clouds are intergalactic in

nature, their metallicities could be $[Z/H] \sim -1$ or lower, but higher metallicities $[Z/H] > -1$ are favored if the clouds are located in the distant Galactic halo since the cloud sizes scale inversely with metallicity. We provide a summary of the HVCs detected in absorption at intermediate resolution with the GHRS and the IUE satellite and find that C IV-HVCs are detected along 3 of 10 extragalactic sight lines down to a level of $\log N(\text{C IV}) \approx 13.3$ (3σ).

Subject headings: galaxies: individual (Markarian 509, PKS 2155-304) – Galaxy: halo – ISM: abundances – ISM: clouds: – radio: lines

1. Introduction

Understanding the properties of high velocity clouds (HVCs) may prove to be an important step in revealing the processes that distribute and ionize gases in the halos of the Milky Way and other galaxies. There have been many ideas proposed to explain the distribution of HVCs on the sky and their kinematics, including supernova-driven expulsion of hot gas into the Galactic halo wherein the gas cools and returns to the disk in a global circulation pattern (i.e., a “Galactic fountain” - Shapiro & Field 1976; Bregman 1980; Norman & Ikeuchi 1989; Houck & Bregman 1990), ram pressure or tidal stripping of material from the Magellanic Clouds (Moore & Davis 1994; Lin, Jones, & Klemola 1995), gas falling into the Milky Way (Oort 1970; Mirabel & Morras 1984), and intergalactic clouds accreting onto the Local Group (Blitz *et al.* 1998). Available data suggest that each of these ideas may be appropriate for some HVCs, but that no single process can adequately describe the character of the entire ensemble of known HVCs (c.f., Wakker & van Woerden 1997).

Many of the same processes that distribute high velocity gases within the Galaxy may also affect the underlying gases of the disk and halo. For example, mass and energy are deposited into the interstellar medium (ISM) by stellar winds and supernovae, which evacuate large regions of the ISM by sweeping up and accelerating interstellar gas (c.f., Spitzer 1990; McKee 1993). Supernovae therefore play a significant role in determining the distribution and ionization of the highly ionized gas in the low halo of the Milky Way (Sembach, Savage, & Tripp 1997; Savage, Sembach, & Lu 1997). At larger distances from the Galactic plane, other processes impacting the properties of HVCs (e.g., tidal effects, interstellar-intergalactic medium interactions, ionization by extragalactic background radiation) may determine the larger scale distributions and physical properties of the gaseous Galactic halo.

Studying gas in the distant halo is observationally challenging since the spectral signature of the gas can be masked by the absorption due to foreground gas in the Galactic disk and low halo. Therefore, studies of HVCs are particularly worthwhile since there is mounting evidence that many HVCs are located within the Galactic halo at large distances from the Galactic plane (c.f., Wakker & van Woerden 1997). By definition, HVCs have observed line-of-sight velocities $|V_{\text{LSR}}| > 100 \text{ km s}^{-1}$, and though this velocity cutoff is somewhat arbitrary, it provides a convenient and historical context in which to classify clouds having velocities significantly exceeding those expected from typical random cloud motions and differential Galactic rotation (Spitzer 1978).

Using the Goddard High Resolution Spectrograph (GHRS) aboard the Hubble Space Telescope (HST), we recently discovered a pair of unusual high velocity clouds in the direction of Mrk 509 ($l = 36.0^\circ$, $b = -29.9^\circ$). These HVCs were detectable only through their C IV absorption signature against the continuum of the Seyfert galaxy. They showed no detectable low ionization (e.g., Si II) absorption or H I 21 cm emission at corresponding velocities (Sembach *et al.* 1995b - hereafter, Paper I), as is usually seen for gases in the disk or low halo of the Milky Way (Sembach & Savage 1992; Savage *et al.* 1997). We called these clouds C IV-HVCs to distinguish them from the H I-HVCs commonly detected in 21 cm emission. Mapping of the H I emission near the Mrk 509 sight line revealed H I-HVCs with similar velocities within $\sim 2^\circ$ of the sight line, which led us to suggest that the C IV-HVCs may be the ionized, extended, low density regions surrounding the H I-HVCs.

The unusual ionization properties of the clouds may provide insight into the properties of the distant Galactic halo, the processes that affect gas at large Galactocentric radii, and the origin(s) of HVCs. Therefore, we initiated a two-part observing program to better understand the properties of the C IV-HVCs. We obtained additional intermediate-resolution GHRS measurements of several ions along the Mrk 509 sight line specifically

to study the ionization conditions in the HVCs in detail. We also identified a pair of C IV-HVCs toward PKS 2155-304 ($l = 17.7^\circ$, $b = -52.2^\circ$) that have ionization properties resembling those of the C IV-HVCs toward Mrk 509..

We report on these new results in this paper, which is organized as follows: In §2 we describe the new observations and data reduction procedures. Section 3 contains the basic interstellar measurements and derived quantities such as ionic column densities. Section 4 is an overview of the high velocity gas in the directions of Mrk 509 and PKS 2155-304. In §5 we model the ionization conditions in the C IV-HVCs, and in §6 we comment on the implications of the ionization results for the thermal pressures of the clouds and their distances. In §7 we discuss the relevance of this work for understanding damped Ly α systems (galaxies) at high redshift. In §8 we present a summary of the intermediate and high velocity gas detections made with the GHRS toward extragalactic objects. Section 9 contains our conclusions.

2. Observations and Reductions

2.1. GHRS Ultraviolet Absorption Line Data

We obtained GHRS intermediate resolution (G160M) observations of PKS 2155-304 and Mrk 509 in October of 1995 and 1996, respectively, as part of HST guest observer programs GO-5889 and GO-6412. A summary of the existing and new observations used in this study is contained in Table 1, where we list the HST identifications, wavelengths covered, dates of observation, detector substepping patterns, on-spectrum integration times, velocity shifts required to put the spectra into a common heliocentric velocity rest frame, and the ISM species detected. The 1257–1293Å spectra for the PKS 2155-304 sight line were kindly provided by Dr. John Stocke (HST program GO-6593). We used the

large ($2.0'' \times 2.0''$) science aperture (LSA) for all observations to reduce slit losses. Unless otherwise indicated, we used standard carousel rotation (FP-SPLIT = 4) and spectrum deflection (comb-addition = 4) procedures to reduce fixed pattern noise structure in each spectrum caused by irregularities in the detector window and photocathode response. We used detector substepping patterns (Step-Patt = 4 or 5) to provide full diode array observations of the off-source backgrounds, which we averaged and subtracted from the on-spectrum data. Substepping pattern 4 provides two substeps per resolution element, which is one diode. We rebinned observations having a sampling interval of four substeps per diode (Step-Patt = 5) to two substeps per diode to improve the signal-to-noise ratio while still satisfying the Nyquist requirement of two independent samples across the 1-diode resolution element.

The post-COSTAR³ LSA observations listed in Table 1 have instrumental profiles with velocity resolutions (FWHM) of approximately 14 km s^{-1} (1550 \AA), 16 km s^{-1} (1400 \AA), and 18 km s^{-1} (1250 \AA). The profiles have a Gaussian core containing $\approx 70\%$ of the light and a broad wing containing $\approx 30\%$ of the light (see Figure 4 of Robinson *et al.* 1998). The 1222–1259 \AA observations of PKS 2155-304 and 1231–1269 \AA observations of Mrk 509 were obtained in 1993 prior to the installation of COSTAR and have a narrow (FWHM $\approx 20 \text{ km s}^{-1}$) core containing $\approx 40\%$ of the spread function area and broad ($\approx \pm 70 \text{ km s}^{-1}$) wings containing approximately 60% of the area. For more information about the performance of the GHRS see Brandt *et al.* (1994) and Heap *et al.* (1995). Technical information about the instrument can be found in Soderblom *et al.* (1994).

³COSTAR is the Corrective Optics Space Telescope Axial Replacement used to correct for the spherical aberration in the HST primary mirror.

2.2. Velocity Determinations

The standard GHRS reduction software produces spectra with absolute wavelength calibrations accurate to approximately ± 1 diode ($\approx 15 \text{ km s}^{-1}$). To obtain more accurate relative velocity scales among the different exposures, we determined relative velocity shifts for the individual Mrk 509 spectra by requiring that the low velocity portions of the low ionization absorption profiles agree in velocity when aligned. The set of Si II lines covered in the individual spectra ($\lambda\lambda 1190.42, 1193.29, 1260.42, 1304.37, 1526.71$) allowed a consistent velocity scale to be determined for all of the Mrk 509 observations, except the integration covering the Si IV region, for which there is no nearby Si II line. Since there was no apparent shift of the low velocity Si IV profiles compared to the C IV profiles (for which we have a simultaneous Si II $\lambda 1526$ measurement), we adopted the default heliocentric velocity scale provided by the standard processing for this observation. Two observations required 10 km s^{-1} shifts with respect to the others, which is within the nominal accuracy of the standard processing. It is particularly important to note that the velocity shift of -10 km s^{-1} determined for the $1300\text{--}1337\text{\AA}$ integration is identical to the shift determined if the low velocity O I $\lambda 1302$, C II $\lambda 1334$, or C II* $\lambda 1335$ absorptions in the same spectrum are used in the low ion comparison instead of Si II $\lambda 1304$ (i.e., there is no velocity “stretch” over the 37\AA interval covered by the observation). The velocities of the Si II line cores in the adopted velocity frame agree well with the velocity of the H I 21 cm emission toward Mrk 509 (e.g., Savage *et al.* 1997). We estimate an accuracy of better than 5 km s^{-1} in the adopted absolute velocities for the Mrk 509 data.

We used the S II $\lambda\lambda 1250, 1253, 1259$ lines to tie the HST observations for PKS 2155-304 into the H I 21 cm emission velocity reference in this direction. The small adjustments made to the velocities ($\approx 5 \text{ km s}^{-1}$) are well within the uncertainties of the velocity scales provided by the standard processing techniques. A comparison of the strong Si II $\lambda 1260$ line with

the Si II $\lambda 1526$ line shows that there are no gross velocity shifts in the longer wavelength data. We estimate an accuracy of $\approx 5\text{--}10 \text{ km s}^{-1}$ in the adopted absolute velocities for the PKS 2155-304 data.

We converted the velocities of all spectra into the Local Standard of Rest (LSR)⁴ by applying shifts $\delta v = 8.9 \text{ km s}^{-1}$ for Mrk 509 and $\delta v = 1.9 \text{ km s}^{-1}$ for PKS 2155-304, where $V_{\text{LSR}} = V_{\text{helio}} + \delta v$. All subsequent velocities in this paper are referenced to the LSR.

In Figure 1 we show the full diode array spectra for the three Mrk 509 observations that have not appeared elsewhere (see Table 1 for references to similar plots of the other spectra used in this study). The individual interstellar lines are identified above each spectrum, as are the high velocity cloud components, when they are sufficiently strong to be visible. Continuum normalized versions of all the interstellar lines identified in the Mrk 509 and PKS 2155-304 spectra listed in Table 1 are shown in Figures 2 and 3.

2.3. H I 21 cm Emission Data for the PKS 2155-304 Sight Line

To complement the HST data for the PKS 2155-304 sight line, we obtained H I 21 cm emission spectra for the sight line and 35 nearby positions using the NRAO 140-foot telescope. The data have an angular resolution of $21'$ and a velocity resolution of 4 km s^{-1} after Hanning smoothing. The locations of these pointings listed in Table 2 are shown in Figure 4. A similar table and map for the Mrk 509 sight line can be found in Paper I. We used a second order polynomial to determine the baseline for each spectrum. In Figure 5

⁴We use the reduction to the LSR given by Mihalas & Binney (1982), which assumes that the Sun is moving in the direction $l = 53^\circ$, $b = 25^\circ$ at a speed of 16.5 km s^{-1} . The LSR conversions for the two directions considered are within 0.5 km s^{-1} of the corrections based on “standard solar motion” frequently used in radio work.

we show the 21 cm spectrum for PKS 2155-304 and several nearby positions where H I is detected at high velocities. Only data for $|V_{\text{LSR}}| > 50 \text{ km s}^{-1}$ are shown because the emission at lower velocities is not completely removed from the spectrum by the $\pm 1.7^\circ$ position switching (on-off source) used to detect the weak, high velocity features. Further details about the observational techniques and data reduction are given by Murphy, Lockman, & Savage (1995).

3. Interstellar Measurements

3.1. Ultraviolet Absorption Lines Toward Mrk 509 and PKS 2155-304

We present the basic interstellar measurements for the Mrk 509 and PKS 2155-304 high velocity clouds in Tables 3 and 4. Continua for all lines were low order (≤ 3) polynomials fitted to featureless continuum regions within several hundred km s^{-1} of the absorption lines. For both sight lines, we divided the HVC absorption into two velocity intervals and made equivalent width and apparent column density estimates based upon integrations within these intervals. The apparent column density is the integral of the apparent column density profile defined by

$$N_a = \int N_a(v) dv = \int \frac{m_e c / \pi e^2}{f \lambda(A)} \tau_a(v) dv = \frac{3.768 \times 10^{14}}{f \lambda(A)} \int \ln \frac{1}{I(v)} dv \text{ [atoms cm}^{-2} \text{ (km s}^{-1}\text{)}^{-1}] \quad (1)$$

where $I(v)$ and $\tau_a(v)$ are the normalized intensity and apparent optical depth at velocity v (see Savage & Sembach 1991 for a discussion of the construction and interpretation of apparent optical depth profiles). The equivalent width and apparent column density errors in Tables 3 and 4 allow for statistical noise in the data and continuum placement uncertainties (see Sembach & Savage 1992). Background uncertainties are minimal ($< 1\%$) in these data since the scattered light properties of the GHRs first-order gratings are excellent (Ebbets 1992).

The C IV-HVCs have the following general properties, as determined by fitting a pair of Doppler-broadened Gaussian absorption components to the $\lambda 1548$ and $\lambda 1550$ lines for each sight line. The fits, which are overplotted on the C IV $\lambda 1548$ lines shown in Figures 2 and 3, are characterized by a central velocity ($\langle V_{\text{LSR}} \rangle$), a Doppler width (b) containing both thermal and turbulent contributions, and a column density (N). The fitted profiles were degraded to the GHRS resolution by convolution with a single Gaussian instrumental profile having $\text{FWHM} = 14 \text{ km s}^{-1}$.

$$\text{Mrk 509:} \quad \langle V_{\text{LSR}} \rangle \approx -283 \pm 3 \text{ km s}^{-1} \quad b \approx 25 \pm 2 \text{ km s}^{-1} \quad \log N(\text{C IV}) \approx 14.10$$

$$\langle V_{\text{LSR}} \rangle \approx -228 \pm 6 \text{ km s}^{-1} \quad b \approx 19 \pm 6 \text{ km s}^{-1} \quad \log N(\text{C IV}) \approx 13.56$$

$$\text{PKS 2155-304:} \quad \langle V_{\text{LSR}} \rangle \approx -256 \pm 7 \text{ km s}^{-1} \quad b \approx 33 \pm 5 \text{ km s}^{-1} \quad \log N(\text{C IV}) \approx 13.50$$

$$\langle V_{\text{LSR}} \rangle \approx -141 \pm 9 \text{ km s}^{-1} \quad b \approx 44 \pm 8 \text{ km s}^{-1} \quad \log N(\text{C IV}) \approx 13.50$$

The column densities derived from the fits are consistent with those obtained by integrating $N_a(v)$ for the weaker C IV $\lambda 1550$ line for PKS 2155-304. However, the values of N_a for the $\lambda 1548$ and $\lambda 1550$ lines for Mrk 509 derived through Eq. (1) indicate that some unresolved saturation is probably present in these profiles. The 2-component Gaussian fits to the lines do not provide much guidance for applying a saturation correction since the inferred b-values are larger than the instrumental function width (14 km s^{-1}), and the S/N of the data do not warrant more complex fits. We note, however, that a Doppler-broadened curve of growth applied to the equivalent widths listed in Table 3 yields column densities for the two components that are about 0.2 dex higher than the fit values or those inferred solely from the weak line results. Given that this saturation correction is (potentially) large and uncertain, we will adopt the weak line N_a values as lower limits in our analysis below.

Measurement of the HVC absorption is straight-forward in all but one case; the Si II $\lambda 1260.422$ HVC feature between -330 and -190 km s^{-1} toward PKS 2155-304 is blended with

low velocity S II $\lambda 1259.519$ absorption. A limit on the amount of Si II HVC absorption within the S II profile can be obtained by comparing the low velocity S II line strength with the two “clean” S II lines at 1250 and 1253Å. A single-component Doppler-broadened curve of growth applied to these equivalent widths, $W_\lambda(1250) = 90 \pm 13$ mÅ and $W_\lambda(1253) = 126 \pm 14$ mÅ, yields a column density of $\log N(\text{S II}) \approx 15.3$. The measured equivalent width of the S II $\lambda 1259$ line is $W_\lambda(1259) = 146 \pm 19$ mÅ. Based on this measurement, the column density derived from the other two S II lines, and the equivalent width errors on all three S II lines, we estimate that < 50 mÅ (2σ) of high velocity Si II is present within the core of the S II $\lambda 1259$ profile. This corresponds to a Si II HVC column density of $\log N(\text{Si II})_{HVC} < 12.86$ (2σ) for a Doppler parameter $b > 5$ km s $^{-1}$.

Table 5 contains a summary of the adopted HVC column densities. These estimates are based on the individual apparent column density measurements listed in Tables 3 and 4. Errors and limits are 2σ estimates. We adopted the conservative approach of quoting lower limits based on weak line results whenever the apparent column densities for multiple lines of a species indicated that a significant saturation correction might be warranted (e.g., C IV toward Mrk 509) or when only a single strong line of an ion was measured (e.g., Si III at -283 km s $^{-1}$ toward Mrk 509). We adopted upper limits based on strong line results whenever a detection was marginal ($\leq 2\sigma$) (e.g., Si IV at -228 km s $^{-1}$ toward Mrk 509 and S II at -256 km s $^{-1}$ toward PKS 2155-304).

3.2. H I 21 cm Observations Toward Mrk 509 and PKS 2155-304

We presented H I 21 cm emission data for the Mrk 509 sight line in Figures 1 and 2 of Paper I. The observing methods, data reduction procedures, and measurement philosophy used in that work were similar to those presented below for the PKS 2155-304 sight line.

Using a deep, frequency switched H I 21 cm emission spectrum for PKS 2155-304, we estimate 4σ upper limits of $\log N(\text{H I}) < 17.73$ for the two C IV-HVCs along the sight line. The baseline RMS of this spectrum is 2.3 mK. We derived estimates of $N(\text{H I})$ for this pointing and the nearby position-switched spectra from the baseline RMS and the following equation:

$$N(\text{H I}) = 1.942 \times 10^{18} \Delta v T_{max} [\text{atoms cm}^{-2}] \quad (2)$$

where Δv is the FWHM of the best fit Gaussian profile in km s^{-1} (assumed to be 30 km s^{-1} when no line is detected), T_{max} is the peak brightness temperature of the line in K (assumed to be 4 times the baseline RMS when no line is detected). In all cases, we assumed the H I is optically thin. Table 2 contains values of T_{max} , Δv (FWHM), $\langle V_{\text{LSR}} \rangle$, and $\log N(\text{H I})$ for 35 positions within $\approx 2^\circ$ of PKS 2155-304.

A schematic map of the positions with velocity information is shown in Figure 4 for the PKS 2155-304 sight line. Filled symbols indicate high velocity gas detections; partially filled symbols indicate that the high velocity gas is broad and spread out in velocity rather than concentrated as a discrete narrow feature; crosses indicate null detections. The numbers to the upper right of the symbols indicate the LSR velocities of the features detected. ^{E1}

4. High Velocity Gas in the Directions of Mrk 509 and PKS 2155-304

There are no known large HVC complexes in the general directions of Mrk 509 or PKS 2155-304. The closest ensemble of clouds to the Mrk 509 sight is the Galactic center negative (GCN) velocity group catalogued by Mirabel & Morras (1984) and Wakker &

^{E1}NOTE TO EDITOR: Editor, please keep Figures 4 and 5 near each other, preferably on the same page.

van Woerden (1991). The GCN clouds generally have peak brightness temperatures several times to an order of magnitude higher than those we measure for the H I-HVCs near the Mrk 509 and PKS 2155-304 sight lines. Some of the known GCN clouds have velocities close to those of H I and C IV-HVCs we detect. For example, in the catalogue of Mirabel & Morras (1984), GCN clouds with $V_{\text{LSR}} = -266$ to -187 km s^{-1} are located within $\sim 5^\circ$ of the Mrk 509 sight line, and a GCN cloud with $V_{\text{LSR}} = -222 \text{ km s}^{-1}$ is located within $\sim 5^\circ$ of the PKS 2155-304 sight line.

The origin of the GCN clouds is unknown, with suggestions ranging from low surface brightness galaxies (Cohen & Mirabel 1978; Mirabel & Cohen 1979) to tidally disrupted gas in the Magellanic Stream in which the gas is flowing in toward the disk near the Galactic center (Mirabel 1981, 1982; Giovanelli 1981; Wakker & van Woerden 1991). The low column density H I-HVCs that we detect near the Mrk 509 and PKS 2155-304 sight lines, which are separated by $\approx 26^\circ$ on the sky, may be characteristic of lower density regions of a larger ensemble of HVCs associated with the GCN clouds.

The H I-HVCs near both the Mrk 509 and PKS 2155-304 sight lines have weak emission, with maximum brightness temperatures of $\sim 50 \text{ mK}$ and $N(\text{H I}) \leq 2 \times 10^{18} \text{ cm}^{-2}$ (two lower velocity clouds near -75 km s^{-1} toward PKS 2155-304 have column densities several times higher). The H I-HVCs near the Mrk 509 sight line have central velocities and widths comparable to those of the higher velocity (-283 km s^{-1}) C IV-HVC. There is no detectable H I at the velocities of the lower velocity (-228 km s^{-1}) C IV-HVC. This situation is reversed for the PKS 2155-304 sight line, where the nearby H I-HVCs occur at velocities somewhat lower than those of the lower velocity (-140 km s^{-1}) C IV-HVC. Figure 5 shows that, in many cases, the H I-HVC detections have widths (FWHM) of $\approx 25\text{--}40 \text{ km s}^{-1}$, similar to the widths of C IV-HVCs ($\approx 30\text{--}45 \text{ km s}^{-1}$). In several pointings, the lower velocity gas is spread out in velocity and no discrete narrow feature is observed (e.g., position B in Figure 5).

The physical connection between the C IV-HVCs and the H I-HVCs is still debatable, though the relative proximity and velocity similarities of the two types of HVCs suggest that they are related. The simplest relationship would be one in which the C IV-HVCs trace the extended, ionized, low density regions of H I-HVCs at large distances from the Galactic plane as suggested in Paper I. Such a situation has been modeled by Ferrara & Field (1994), who considered the ionization structure of clouds in a hot Galactic halo subjected to extragalactic background radiation. Their model predicts a core-interface structure for various combinations of the total hydrogen column density and the linear size of the cloud (see their Figure 6). In their model, the cloud core consists primarily of neutral gas (perhaps H I-HVCs), while the interface region between the core and the surrounding hot gas (perhaps C IV-HVCs) is ionized primarily by photoionization by the extragalactic background. Thermal conduction and shocks could also be important factors in establishing the ionization conditions in such situations.

Wolfire *et al.* (1995) also considered the thermal and ionization structures of clouds embedded in a hot Galactic halo. They found that a stable two-phase neutral gas structure consisting of cold, neutral cloud cores and warm, neutral cloud envelopes exist over a narrow range of pressures at a given height from the Galactic plane. The cold cores exist only for $z \leq 20$ kpc. There is no convincing evidence in the ultraviolet absorption line data for cold cores in the C IV-HVCs toward Mrk 509 or PKS 2155-304. The strengths and widths of the H I-HVC profiles are more suggestive of warm, low density gas than cold cores. This is consistent with a location for the C IV-HVCs at large distances from the Galactic plane.

Benjamin & Danly (1997) recently proposed a simple model of Galactic infall in which low density H I-HVCs have velocities determined primarily by the drag forces between the clouds and the warm and hot gases of the Galactic halo. In such a model, the terminal velocity of a HVC, v_T , is related to the observed velocity through the simple relation $v_T =$

$v_{obs} \csc |b|$. The velocities of the C IV-HVCs toward Mrk 509 are probably too high to be explained by this simple model since the values of v_T ($\approx 450\text{--}550 \text{ km s}^{-1}$) are comparable to the Galactic escape velocity of $\approx 500 \text{ km s}^{-1}$ (Binney & Tremaine 1987). The implied distances for the clouds in this simple model are so large that the assumptions used in the Benjamin and Danly analysis are invalid. [A similar conclusion is obtained if one attributes some of the peculiar velocity to Galactic rotation since large velocities ($V_{LSR} \leq -80 \text{ km s}^{-1}$) are reached only for very large distances ($d > 45 \text{ kpc}$)]. A similar conclusion holds for the PKS 2155-304 sight line, though the observed velocities are smaller. The large negative velocities of the GCN clouds in this part of the sky led Mirabel & Morras (1984) to conclude that the HVCs are probably infalling gas clouds located at large distances from the Galactic plane.

5. Ionization of the C IV-HVCs

With the HST, it is feasible to use QSOs and active galactic nuclei (AGNs) as background sources for HVC absorption line studies. Our present study of the Mrk 509 C IV-HVCs provides the most complete ionic information available for high velocity clouds outside the Galactic disk.

The absorption line signatures of the C IV-HVCs toward Mrk 509 and PKS 2155-304 are unlike those of most sight lines through the Galactic disk and low halo. Low velocity ($|V_{LSR}| < 100 \text{ km s}^{-1}$) gas in the Galactic disk and low halo is generally characterized by strong low ionization absorption in addition to high ion absorption (see Figures 2 and 3). The strong Si II $\lambda\lambda 1526, 1260$ lines and the C II $\lambda 1334$ line are usually much stronger than either the Si IV $\lambda\lambda 1393, 1402$ or C IV $\lambda\lambda 1548, 1550$ lines. $N(\text{C IV})/N(\text{C II}) > 1$ in the C IV-HVCs, compared to $\ll 1$ in the Galactic disk and halo. Furthermore, the C IV-HVCs have $N(\text{C IV})/N(\text{Si IV}) > 5$ and $N(\text{C IV})/N(\text{N V}) > 5\text{--}10$, while gas within the disk or low

halo typically has $N(\text{C IV})/N(\text{Si IV}) \approx 3.8 \pm 1.9$ and $N(\text{C IV})/N(\text{N V}) \approx 4.0 \pm 2.4$ (Sembach *et al.* 1997). Strong departures from these average high ion ratios are generally observed only for sight lines that pass through known radio continuum loops, and in one case high values are found for an extended interarm region (Sembach 1994). The combination of unusual high ionization ratios coupled with the absence of low ionization absorption is also atypical of high velocity gases in the Vela supernova remnant (Jenkins, Wallerstein, & Silk 1976, 1984) or star-forming regions like Carina (Walborn *et al.* 1998). To a large degree, the C IV-HVCs resemble the low column density ($\log N(\text{H I}) < 17$) QSO metal line absorption systems, in which one often sees strong C IV (and sometimes Si IV) absorption but little low ionization absorption (Steidel 1990; Songaila & Cowie 1996).

Photoionization by Extragalactic Background Radiation

Given that the C IV-HVCs are likely to be at large distances from the Galactic plane, we explored their ionization properties assuming that the dominant ionization mechanism within the gas is photoionization by extragalactic radiation due to the integrated light of QSOs and AGNs. Using the photoionization code CLOUDY (v90.02; Ferland 1996), we modeled the HVCs as plane-parallel slabs of gas bathed from both sides in extragalactic background radiation with the QSO spectral energy distribution given by Madau (1992) and a mean intensity at the Lyman limit $J_\nu(\text{LL}) = 1 \times 10^{-23} \text{ erg cm}^{-2} \text{ s}^{-1} \text{ Hz}^{-1} \text{ sr}^{-1}$ (Donahue, Aldering, & Stocke 1995; Haardt & Madau 1996). This corresponds to an ionizing photon density $n_\gamma = 4.3 \times 10^{-7} \text{ ph cm}^{-3}$. We ignored the effects of intervening clouds on the shape of the spectral energy distribution, and we assumed that the clouds had a uniform gas density. We scaled the elemental abundances in the model to an overall metallicity, $[Z/H]$, relative to the solar system abundances given by Anders & Grevesse (1989), though the differential elemental abundance pattern in the model remained constant (i.e., we assumed

no dust or local nucleosynthetic enrichment effects).⁵

The ionization structure of a cloud in which the ionization is photon dominated is essentially determined by the ionization parameter [$\Gamma = (n_\gamma/n_H) \propto (J_\nu/n_H)$], the ratio of ionizing photon density to total gas density (Bergeron & Stasinska 1986). For clouds that are optically thin [$\tau_{LL} < 1$ or $\log N(\text{H I}) < 17.2$], a few scaling laws apply for fixed values of Γ .

$$N(Z) \propto (Z/H) \times N(\text{H I})$$

$$N(\text{H I}) \propto n_{HI} \times D$$

$$n_{HI} \propto n_H \times (n_H/J_\nu)$$

where D is the cloud size. Strictly speaking, the scaling laws are only approximate and depend on the metallicity of the gas, which affects the temperature of the gas and hence the ionization balance. For $[Z/H] < 0$, the above approximations are adequate for our purposes. The scaling laws become almost exact at $[Z/H] < -1$ when metal cooling becomes less efficient. At $\log N(\text{H I}) > 17.2$ ($\tau(\text{LL}) > 1$), the clouds become self-shielded and the scaling laws break down. We note that the present epoch value of $J_\nu(\text{LL})$ is still uncertain. Since the ionization structure of the gas depends only on Γ , a change in $J_\nu(\text{LL})$ does not affect the relative column densities of the ions as long as the total gas density is changed accordingly. For example, when $J_\nu(\text{LL})$ is lowered by a factor of 2, the ionization structure (e.g., C I : C II : C III : C IV) of the gas is unchanged if the gas density is also lowered by a factor of 2. If the density is lowered, the absolute column densities will also be lowered unless the cloud size is increased accordingly.

⁵We use the square-bracketed quantity $[Z/H]$ to indicate the logarithm of metal abundances relative to solar abundances: $[Z/H] = \log(Z/H) - \log(Z/H)_\odot$.

We computed a set of models with various values of $\log N(\text{H I})$ and $[Z/\text{H}]$ to determine the optimal set of parameters that satisfy the observed column densities and column density limits of the ions in the C IV-HVCs toward Mrk 509 and PKS 2155-304. In Figure 6 we plot the results of one such model for the Mrk 509 C IV-HVCs at -283 km s^{-1} (left panel) and -228 km s^{-1} (right panel). The symbols correspond to different ions as defined in the figure legend. The solid lines connecting the symbols indicate the ranges of $\log \Gamma$ (or $\log n_H$) that satisfy the individual observed ionic column density measurements and limits. The heavy vertical line in each panel indicates the value of $\log \Gamma$ (or $\log n_H$) that satisfies all of the observed column density constraints simultaneously. For the -283 km s^{-1} cloud we find that a value of $\log \Gamma \approx -2.55$ ($\log n_H \approx -3.82$) for a model with $\log N(\text{H I}) = 16.3$ and $[Z/\text{H}] = -0.5$ satisfies the detections and upper limits over a very narrow range in Γ . The main observational constraints are provided by C II, C IV, Si IV, and N V (see Figure 6). For the -228 km s^{-1} cloud we find that a slightly larger value of $\log \Gamma \approx -1.90$ ($\log n_H \approx -4.48$) for a model with $\log N(\text{H I}) = 14.7$ and $[Z/\text{H}] = -0.5$ marginally satisfies all of the observable constraints. For this cloud, the Si III column density provides a significant additional constraint. In both cases, the metallicities can be varied provided that the relative ionic column densities are maintained by adjusting $N(\text{H I})$ according to the approximate scaling laws listed above.⁶

The cloud sizes in the standard models discussed above with $[Z/\text{H}] \approx -0.5$ range from roughly 4 to 30 kiloparsecs. Lower metallicity models imply larger cloud sizes and somewhat larger temperatures than the solar metallicity models. We can reasonably eliminate metallicities $[Z/\text{H}] < -2.0$ since the implied cloud size for the -283 km s^{-1} C IV-HVC toward Mrk 509 would be ≥ 500 kiloparsecs. Within the context of the photoionization models,

⁶In other words, a model with $\log N(\text{H I}) = 16.8$ and $[Z/\text{H}] = -1$ yields approximately the same metal line column density results as one with $\log N(\text{H I}) = 16.3$ and $[Z/\text{H}] = -0.5$.

$[Z/H] > -1$ is favored if the clouds are associated with the Milky Way (i.e., in the distant Galactic halo). An intergalactic location for the clouds would allow for lower metallicities.

The amount of C IV in the HVCs toward PKS 2155-304 is about an order of magnitude lower than the amount observed in the higher velocity HVC toward Mrk 509. The available data indicate that these C IV-HVCs can be modeled successfully with parameters similar to those used for the Mrk 509 C IV-HVCs. For example, both clouds can be modeled with the standard parameters used for the -283 km s^{-1} HVC toward Mrk 509 provided that the ionization parameter is lower, $\log \Gamma \approx -3.00$ ($\log n_H \approx -3.38$). Figure 7 contains the model results for the PKS 2155-304 C IV-HVCs. Both clouds can also be adequately represented with lower column density models like those for the -228 km s^{-1} cloud toward Mrk 509 provided that $\log \Gamma \approx -2.20$ ($\log n_H \approx -4.18$). Observations of additional ions along the PKS 2155-304 sight line would help to characterize these clouds more completely.

This study refines our earlier estimates of the ionization conditions within the C IV-HVCs toward Mrk 509 (Paper I). The range of acceptable models available with the earlier data is now much more tightly constrained, and our original conclusion that these clouds are probably large, low density, highly ionized regions remains intact. Our new observations have allowed us to quantify these statements more fully and to determine that the two C IV-HVCs along the sight line may have different ionization properties. These differences are most likely due to differences in gas density rather than to viewing angle or partial shielding of one cloud by another since the optical depths of the clouds are small (< 1). This may also explain why some HVCs at large distances from the Galactic plane have no detectable C IV absorption. If the gas density becomes too high, little C IV is created. For example, HVC287.5+22.5+240 has no detectable C IV absorption, and interferometric H I data show a concentrated cloud directly along the sight line, with $N(\text{H I}) = 8 \times 10^{19} \text{ cm}^{-2}$ (Lu *et al.* 1998; Wakker *et al.* 1998).

In the above discussion we have not considered the effects of a non-solar relative abundance pattern that might result if dust is present within the HVCs. Clear evidence for dust in a (presumably) distant HVC along the NGC 3783 sight line has recently been found by Lu *et al.* (1998). Of the elements considered in our study, Si would be most affected by gas-phase depletion onto dust grains. The depletion of C, N, and S onto dust grains is expected to be very small (less than a factor of 3) in these types of environments (Savage & Sembach 1996). An intrinsic non-solar relative abundance pattern could also affect our conclusions. For example, the abundance pattern may be similar to that seen for metal-poor halo stars, in which Si is slightly overabundant relative to C and N by a factor of ≈ 2 (Wheeler, Sneden, and Truran 1989). For the Mrk 509 clouds, a super-solar metallicity of $[Z/H] \sim 0.7\text{--}1.0$ and a silicon gas-phase depletion relative to carbon $[\text{Si}/\text{C}] \sim 1.0$ allows values of $\log \Gamma$ as low as ≈ -2.95 ($\log n_H \approx H - 3.43$) for the -283 km s^{-1} cloud and ≈ -2.68 ($\log n_H \approx H - 3.70$) for the -228 km s^{-1} cloud. These values of Γ are roughly 3–6 times higher than the values in the “standard” models discussed above but do not significantly change the main conclusions of this paper. We present a summary of the properties of the C IV-HVCs toward Mrk 509 derived from these photoionization models in Table 6.

Photoionization by Starlight

An additional source of ionizing photons that was not considered in the previous section is the integrated light emitted from hot stars within the Galaxy. The subject of how photons from O-stars affect the ionization properties of the diffuse ionized gas (DIG) in the ISM has been studied recently by several groups, who find that a sufficient number of photons may leak out of the Galactic disk to ionize the “Reynolds Layer” (Miller & Cox 1993; Domgörgen & Mathis 1994). The fraction of photons that escape from the disk into the halo at a given Galactocentric radius depends upon the ionization, porosity, and dust distribution within the ISM, as well as the adopted number and distribution of hot

stars in the Galaxy. Dove & Shull (1994) estimate an average number of Lyman continuum photons escaping through both the Galactic H I layer and the top of the DIG layer to be $\Phi_{LyC}(\ast) \approx 1.5 \times 10^6 \text{ cm}^{-2} \text{ s}^{-1}$. Measurements of the H α emission from high velocity clouds in Complexes A, C, and M imply $\Phi_{LyC}(\ast) \approx (1.3\text{--}4.2) \times 10^5 \text{ cm}^{-2} \text{ s}^{-1}$ if the emission arises from photoionization of the clouds (Tuftte, Reynolds, & Haffner 1998). All three complexes lie several kiloparsecs from the Galactic plane (see Wakker & van Woerden 1997). These estimates are larger than the Lyman continuum flux from the extragalactic background in our photoionization model ($\Phi_{LyC}(\text{EB}) \approx 1.27 \times 10^4 \text{ cm}^{-2} \text{ s}^{-1}$) and suggests that internal Galactic sources contribute to the ionization properties of gas in the low Galactic halo.

A pure stellar ionizing spectrum of the type ionizing the DIG ($T_{eff} \approx 38,000 \text{ K}$; Domgörgen & Mathis 1994) does not produce enough C IV to match the C IV to Si IV ratios measured in the C IV-HVCs. The amount of Si IV relative to C IV would be about an order of magnitude higher than observed unless Si is more heavily depleted onto dust grains than C by a similar factor (Giroux & Shull 1997 see their Figure 4). Also, the amount of doubly ionized ions, such as Si III, relative to C IV in such a model is expected to be considerably larger than is observed (see Bregman & Harrington 1983). To further explore the effects of a harder radiation field than that of the DIG but softer than that of the pure QSO power law spectrum, we recalculated our photoionization models with a QSO spectrum filtered by intervening clouds (Haardt & Madau 1996) combined with a $T_{eff} = 50,000 \text{ K}$ stellar spectrum having $J_{\nu}(\text{LL}) \sim 10^{-22} \text{ erg cm}^{-2} \text{ s}^{-1} \text{ Hz}^{-1} \text{ s}^{-1}$. The intensity at the Lyman limit due to the stellar portion of the spectrum is about 10 times higher than that of the extragalactic background contribution. The resulting ionizing spectrum has a small break at the Lyman limit and a large break at 4 Rydberg. This hybrid model can reproduce the observed ionic column densities for the -283 km s^{-1} cloud only if $\log \Gamma \approx -2.0$, which is comparable to the value required for the pure QSO power law spectrum. For the -228 km s^{-1} cloud toward Mrk 509, it is necessary to incorporate a Si/C

depletion of about 0.5 dex to make the model match the observed column densities. We plot these results for the Mrk 509 C IV-HVCs in Figure 8. Acceptable hybrid models yield physical parameters for the clouds similar to those listed in Table 6.

Collisional Ionization

An alternative production mechanism for the ionized species in the Mrk 509 C IV-HVCs is collisional ionization within a hot plasma. There are a host of predictions for the column densities expected under various collisional ionization situations, including turbulent mixing of cool and hot gases in shear flows (Shull & Slavin 1994), magnetic conductive interfaces (Borkowski, Balbus, & Fristrom 1990), supernova bubbles in late stages of evolution (Slavin & Cox 1992, 1993), and radiatively cooling flows (Benjamin & Shapiro 1998). A recent review of these hot gas theories and their relevance to production of highly ionized gases in the disk and halo has been given by Sembach *et al.* (1997). The most highly ionized gas lines observed in our study (Si IV, C IV, and N V) cannot be used alone to completely rule out a collisional ionization origin for the C IV observed in the HVCs toward Mrk 509 and PKS 2155-304. However, the absence of significant low ionization absorption associated with the high ion detections indicates that a collisional ionization origin for most of the ionized gas is unlikely. Except under special circumstances, all of these collisional ionization models predict that some low ionization gas will be present along with the hot gas, and several of these by their very nature have spatially coincident regions of hot and cool gases.

In Table 7 we compare the ionic ratios observed for the two C IV-HVCs toward Mrk 509 with typical values found for the low disk and halo, values predicted for a hot ($T_{max} = 10^6$ K) radiatively cooling gas, and values predicted for the extragalactic background photoionization models discussed above. Only a few of the observed constraints can be satisfied by the radiatively cooling gas calculations, whereas the photoionization models satisfy all of the listed ratios (as well as others that are not listed). One caveat to

bear in mind before eliminating collisional ionization for the C IV-HVCs is that the gas may be very hot ($T > 5 \times 10^5$ K) and not yet have had time to cool and recombine to produce the lower ion species. The ionization fractions of the singly ionized species observed depend strongly upon the assumed stopping point in the cooling flow calculations (see Benjamin & Shapiro 1998).

Future observations of the Mrk 509 and PKS 2155-304 sight lines would be valuable for further discrimination among the various ionization scenarios for the C IV-HVCs. The Far Ultraviolet Spectroscopic Explorer (FUSE) will observe both sight lines within the next few years. The FUSE bandpass (905–1195Å) includes the O VI $\lambda\lambda 1031, 1037$ doublet, which is the best diagnostic of hot ($> 10^5$ K) collisionally ionized gas in the ultraviolet spectral region.⁷ Most collisional ionization models predict $N(\text{O VI})/N(\text{C IV}) > 1$ if the gas is hot (Sembach *et al.* 1997), though some turbulent mixing layer models allow lower values if the post-mixed gas temperature in the cooling flow is not too high (Shull & Slavin 1994). If the absence of low ionization gas in the C IV-HVCs is due to high temperature collisional ionization, the O VI absorption should be strong. In the pure power law photoionization models considered here, the predicted O VI column density is comparable to that predicted for N V and is about an order of magnitude lower than the C IV column density (see Figures 6 and 8). The predicted O VI column densities are much less in the hybrid QSO/stellar spectrum models considered. Therefore, distinguishing between the observational signatures of hot collisionally ionized gas and photoionized gas in the C IV-HVCs should be feasible.

⁷The ionization potential of O VI is 113.9 eV, compared to 47.9 eV for C IV and 77.5 eV for N V (Moore 1970).

6. On the Origin and Distances of the C IV-HVCs

The results of our investigation into the ionization properties of the C IV-HVCs in the previous section lead to two important conclusions. First, it appears that the principal ionization mechanism is photoionization by light with a relatively hard (QSO-like) spectrum, though some contributions due to collisional ionization or a relatively hot stellar-like spectrum are possible. Second, the derived thermal pressures in the photoionization models are very small, $P/k \sim 2 \text{ cm}^{-3} \text{ K}$, compared to typical interstellar thermal pressures of $\approx 2000\text{--}3000 \text{ cm}^{-3} \text{ K}$ in the Galactic disk. Both conclusions lead us to believe that the C IV-HVCs are associated with intergalactic gas in the Local Group or very distant gas in the Galactic halo.

A simple argument in favor of a large distance for the C IV-HVCs can be made by considering the properties of the H I-HVCs near the Mrk 509 sight line. The thermal pressure in the H I-HVCs is given by $P/k = n_{HI}T$, where n_{HI} is the total neutral gas density and T is the temperature of the clouds. The pressure will be larger if the gas in the H I-HVCs is partially ionized. The pressure can be recast as an equation for distance given by $d = \text{size} / \theta = (N(\text{H I})/n_{HI}) / \theta = (P/k)^{-1} (T/\theta) N(\text{H I})$, where θ is the angular extent of a spherical cloud in radians. The widths of the H I profiles for the H I-HVCs indicate that $T < 2 \times 10^4 \text{ K}$, but a more realistic estimate of the temperature can be made by requiring that it be less than the temperature derived for the highly ionized gas regions, $T \leq 10^4 \text{ K}$. Adopting a temperature of $T \approx 10^4 \text{ K}$, a typical column density of $N(\text{H I}) = 2 \times 10^{18} \text{ cm}^{-2}$, and conservative (large) angular size $\theta \approx 2^\circ$ (see Paper I), we find that $d(\text{kpc}) \approx 185 (P/k)^{-1}$. Assuming rough thermal pressure equilibrium between the C IV-HVCs and the H I-HVCs yields $d \approx 30\text{--}200 \text{ kpc}$. Smaller values of θ increase this estimate, while smaller values of T decrease it. If the pressure in the H I emitting gas is larger than estimated above due to ionization effects, the distance will decrease.

The C IV-HVC properties are roughly consistent with a core-interface (H I – C IV) structure in the model proposed by Ferrara & Field (1994). Such clouds would have to be located at large distances from the Galactic plane for the extragalactic radiation field to dominate their ionization characteristics. The implied thermal pressures for the C IV-HVCs are much smaller (2–3 orders of magnitude) than those predicted for multi-phase models of the Galactic halo at $|z| < 10$ kpc (e.g., Wolfire *et al.* 1995). The C IV-HVC pressures can also be compared to the pressure expected for an extended Galactic corona. An estimate of gas density at very large distances from the Galactic plane follows from the detection of H α emission from the Magellanic Stream (Weiner & Williams 1996). If the observed H α emission is produced by ram pressure heating as the Magellanic Stream moves through a hot Galactic corona, the detections provide information about the conditions in the corona at ~ 50 kpc from the Galactic plane. The Weiner & Williams analysis implies that the coronal gas has $T \sim 1.7 \times 10^6$ K with $n_H \sim 1 \times 10^{-4}$ cm $^{-3}$ and $P/k = 2.3n_H T \sim 390$ cm $^{-3}$ K, two orders of magnitude larger than the C IV-HVC thermal pressures. (The factor of 2.3 arises from the assumption that the gas is fully ionized and contains 10% He by number.)

Given the large inferred pressures and ionization signature for the C IV-HVCs it is interesting to consider the possibility that the C IV-HVCs are intergalactic clouds rather than entities within the Galactic halo. Giovanelli (1981) argued that much of the GCN HVC complex (to which the C IV-HVCs may be related) was probably not part of a population of intergalactic clouds based upon the cloud velocities and turbulent motions within the clouds; he assigned them to gas associated with tidal debris from the Magellanic Stream. However, Blitz *et al.* (1998) recently considered the intergalactic origin hypothesis in more detail and suggested that when a larger ensemble of HVCs is considered, some HVCs may be more properly considered members of the Local Group than clouds within the Milky Way. They base this conclusion on the velocity centroid of the restricted HVC cloud ensemble considered; this centroid has the same kinematical radial velocity centroid

as the Local Group. However, not all HVCs fit well into the Blitz *et al.* model, including the Magellanic Stream and Complexes A, C, and M. HVC 287.5+22.5+240 fits the kinematical and positional aspects of the model, but it has a metallicity, $[S/H] = -0.6$, that is too high to be consistent with a primordial gas cloud (Lu *et al.* 1998). Still, many of the C IV-HVCs properties suggest that an intergalactic location for some HVCs may be possible. In this context, it is important to note that the C IV-HVCs contain metals.

If the C IV-HVCs are indeed intergalactic clouds, then the metallicity constraint of $[Z/H] > -1$, which was derived in §5 under the assumption that the clouds are located in the distant Galactic halo and have sizes no larger than a few tens of kiloparsecs, may be relaxed. Observations of absorption lines along closely paired lines of sight toward quasars show that low redshift ($z \sim 0.7$) Ly α clouds have extents of ~ 500 kiloparsecs (Dinshaw *et al.* 1995). If the C IV-HVCs are of similar nature and size, then metallicities of $[Z/H] < -1$ may be allowed.

The derived properties of the C IV-HVCs are consistent with the properties found for the high redshift ($z \sim 3$) Ly α clouds; for a sample of about 30 clouds, Songaila & Cowie (1996) find that $N(\text{C IV})/N(\text{H I}) \approx 2 \times 10^{-3}$ and $\log \Gamma \approx -1.9$ for $10^{14} < N(\text{H I}) < 10^{15} \text{ cm}^{-2}$, and $N(\text{C IV})/N(\text{H I}) \approx 3 \times 10^{-3}$ and $\log \Gamma \approx -2.5$ for $10^{15} < N(\text{H I}) < 10^{17}$. According to recent cosmological simulations of structure formation involving gas hydrodynamics (Petitjean, Mucket, & Kates 1995; Zhang, Anninos, & Norman 1995; Hernquist *et al.* 1996; Miralda-Escudé *et al.* 1996), Ly α clouds at $2 < z < 4$ with $10^{14} < N(\text{H I}) < 10^{17} \text{ cm}^{-2}$ trace the diffuse gas in the filamentary and sheet-like structures that surround and connect galaxies. The simulations indicate that the gas in the sheets and filaments gradually become denser concentrations that eventually form galaxies. It is not unreasonable to think that some of this gas may have survived to the present day. The C IV-HVCs and some of the H I-HVCs may be manifestations of such filamentary structures within the nearby universe

(see Blitz *et al.* 1998).

7. Comparisons with High Redshift Galaxies

One of the main motivations for studying the distribution and physical properties of gas in the Galactic disk and halo is to understand the origin of intervening metal absorption line systems found in spectra of quasars at high redshifts. In this regard, a comparison of the absorption properties of the Milky Way with those of the QSO damped Ly α (DLA) systems may be particularly relevant since the latter are thought to arise from the high redshift counterparts of present-epoch galaxies and may possibly be the progenitors of spiral galaxies (Wolfe *et al.* 1986; Prochaska & Wolfe 1997b). Such a comparison was carried out recently by Savage *et al.* (1993a), who compared the equivalent width distributions of high and low ion absorption lines from the Milky Way toward extragalactic sight lines with those from DLA systems at a mean redshift $\langle z \rangle = 2.4$. Although there are several factors that can bias the comparisons and influence the observed character of the absorption line system (see Savage 1988), the low ion absorption lines arising from the Milky Way disk and halo seem to have an equivalent width distribution similar to most DLA systems. However, Savage *et al.* noted that the differences in the high ion absorption lines are more acute in that the C IV and Si IV absorption from the Galaxy is significantly weaker on average than that found in DLA systems (see their Figure 10). These comparisons reveal primarily the differences in the kinematics of the gas rather than differences in heavy element abundances since most of the absorption lines involved in the comparisons are saturated. Indeed, we now know that DLA systems at $\langle z \rangle \approx 2.4$ generally have metallicities a factor of 10–100 below solar (c.f., Pettini *et al.* 1997; Lu *et al.* 1996).

The increasing availability of high resolution observations of DLA absorption systems allows direct comparisons of the absorption line profiles of various species and the gas

kinematics in the DLA systems and the Milky Way. This provides more information than simple equivalent width measurements. In particular, echelle observations carried out with the Keck 10m telescopes (Wolfe *et al.* 1994; Lu *et al.* 1996; Prochaska & Wolfe 1996, 1997a) show that C IV and Si IV absorption lines in DLA systems generally have profiles very different from those of low ionization species in both the component structure and the velocity extent of the absorption. This apparent dis-jointedness between high and low ionization characteristics was interpreted by those authors to mean that most of the high ion gas in DLA systems arises from regions that are physically distinct from the low ion gas, possibly from low density, ionized gaseous halos surrounding the neutral gas concentration. In comparison, the high ion (C IV and Si IV) and low ion absorption lines in the Galactic disk and low halo tend to have roughly similar absorption profiles and velocity extents (Sembach & Savage 1992; Savage *et al.* 1993b). The properties of the C IV-HVCs may shed new light on the issue. The C IV-HVCs by definition, occur at velocities beyond those where disk and low halo gas absorption is usually seen and show relatively strong high ion absorption with little or no detectable low ion absorption. In this regard, the C IV-HVCs toward Mrk 509 and PKS 2155-304 are qualitatively similar to those of DLA absorption line systems. Quantitatively, there are still large differences between the average Galactic absorption and DLA absorption, mainly because the covering fraction of Galactic sight lines with C IV-HVCs is small (see §8). The difference could be due to (possibly) greater rates of gas infall and a higher extragalactic ultraviolet radiation field intensity at high redshift.

8. A Summary of High and Intermediate Velocity Gas Toward Extragalactic Objects

Data from previous investigations of halo gas along extragalactic sight lines can be used to inventory the types of high velocity clouds encountered along complete paths through

the Galactic disk and halo. Savage & Sembach (1996) and Wakker & van Woerden (1997) have compiled lists of H I-HVC metal line detections. Here, we provide a comparison of some of these results with detections / non-detections of highly ionized species. We have summarized the HVC detections in Table 8, where we indicate whether the HVCs have been detected in H I emission, low ion absorption, and C IV absorption. Cases of HVC detections in the low ionization lines that have not had an integration to search for the presence of C IV are not considered here. When possible, we have assigned the high velocity gas detections to identified HVCs or cloud complexes. Details about the individual detections / non-detections can be found in the references cited in Table 8.

8.1. High Velocity Clouds (HVCs)

In the sample of objects that have high quality high ionization data obtained at intermediate resolutions with the GHRS or International Ultraviolet Explorer (IUE) satellite we find:

- 1) Three sight lines with C IV-HVCs, weak low ionization absorption, and no detectable high velocity H I 21 cm emission (Mrk 509, PKS 2155-304, and H 1821+643 at $V_{\text{LSR}} = -213 \text{ km s}^{-1}$). For both the Mrk 509 and PKS 2155-304 sight lines there is high velocity H I 21 cm emission within 2 of the sight lines (see §4). The vicinity of the H 1821+643 sight line has not yet been sensitively searched for low column density H I-HVCs.
- 2) One case of high velocity C IV absorption possibly associated with the H I warp of the outer Galaxy (H 1821+643 at $V_{\text{LSR}} = -120 \text{ km s}^{-1}$). H I 21 cm emission and strong low ion absorption are present over the velocity range covered by the C IV absorption.
- 3) One H I-HVC detected in both H I 21 cm emission and strong low ion absorption, with possible C IV absorption at the 2.7σ level (Fairall 9). In this case the HVC is a portion of

the Magellanic Stream.

4) Two cases of H I-HVCs seen in both H I 21 cm emission and low ionization absorption with no detectable C IV absorption to a 3σ level of $\log N(\text{C IV}) \leq 13.33$ (Mrk 205 and NGC 3783).

5) Three cases where there are no obvious H I or C IV-HVCs (3C 273, NGC 3516, NGC 5548). These sight lines pass through very different regions of the Galaxy. The 3C 273 sight line is a high latitude direction that passes through Loop I and near the edge of Loop IV. Intermediate velocity gas exists along the sight line, though some of the negative gas velocities are undoubtedly due to differential Galactic rotation (see Savage *et al.* 1993b). The NGC 3516 sight line is a moderate latitude direction that passes through Loop III near HVC Complex C. The NGC 5548 sight line is a high latitude direction that passes within 20° of the North Galactic Pole.

6) Numerous cases where high positive velocity absorption is seen in both low ionization and high ionization gas that is clearly associated with the LMC near $+270 \text{ km s}^{-1}$ and the SMC near $+150 \text{ km s}^{-1}$. The three best studied cases with the IUE satellite include HD 5980 in the SMC and HD 36402 and SN 1987A in the LMC. GHRS results for C IV and Si II have been published for two LMC stars by Bomans *et al.* (1996). The 270 km s^{-1} velocity separation between the LMC and the Milky Way absorption permits a search for high velocity gas associated with the Milky Way in the velocity range from approximately $+100$ to $+150 \text{ km s}^{-1}$. de Boer *et al.* (1990) concluded that the absorption extending over this velocity range is not associated with the LMC. While a location for this gas in the outer halo of the Milky Way is a distinct possibility, the kinematic complexity of Magellanic Cloud and Magellanic Stream gas along these directions makes it difficult to draw unambiguous conclusions.

7) The inner Galaxy sight line to the star HD 156359, ($l = 328.7^\circ$, $b = -14.5^\circ$, $d = 11.1$

kpc, and $z = -2.8$ kpc), which has a HVC at $+125 \text{ km s}^{-1}$ detected in C II, Mg II, Si II, Si III, and Fe II with the IUE (Sembach, Savage, & Massa 1991) and in Si II and N V with the GHRS (Sembach, Savage, & Lu 1995a). In the direction of HD 156359, Galactic rotation should produce velocities ranging from 0 to -100 km s^{-1} , while the HVC has a large positive velocity. In this particular case, the HVC was not detectable in the lines of C IV or Si IV with the IUE. The observations provide the constraints $N(\text{C IV})/N(\text{N V}) < 3.4$ and $N(\text{Si IV})/N(\text{N V}) < 0.9$.

In all cases where the extragalactic sight line passes through a known H I-HVC detected through H I 21 cm emission observations, ultraviolet low ionization absorption is present. This result is not surprising since there has been no evidence for primordial (highly metal deficient) H I high velocity gas clouds falling into the Milky Way. The observations noted here cover a wide range of Galactocentric distances and angular scales.

8.2. Intermediate Velocity Clouds (IVCs)

Intermediate velocity ($30 < |V_{\text{LSR}}| < 100 \text{ km s}^{-1}$) gas exists along many of the extragalactic sight lines that have been observed with the GHRS. Some of the more relevant cases for comparison with the high velocity gas include:

- 1) Two H I-IVCs with C IV absorption at similar velocities (Mrk 205, NGC 3516). In both cases, the C IV absorption may be due to a broader velocity distribution of high ion gas. Component by component matching of the C IV absorption to the H I emission is less clear than in the high velocity cases.
- 2) One case of intermediate velocity C IV absorption at $V_{\text{LSR}} = -70 \text{ km s}^{-1}$ that may be associated with the high- $|z|$ extension of the Perseus spiral arm (H 1821+643). H I 21 cm emission and low ion absorption are also seen at the velocities of the C IV absorption.

3) Intermediate velocity ($\sim 60\text{--}90\text{ km s}^{-1}$) absorption in C IV, Si IV, and lower ionization stages along most LMC sight lines observed with the IUE (Savage & de Boer 1981; Chu *et al.* 1994; Bomans *et al.* 1996).

8.3. 8.3. Sky Coverage

Murphy *et al.* (1995) found that approximately 37% of sky is covered by H I-HVCs down to a detection limit of $\log N(\text{H I}) \approx 17.7$ (5σ). Using the GHRS data for the extragalactic sight lines listed in Table 8, not including the LMC and SMC directions, we find C IV detections having $\log N(\text{C IV}) > 13.3$ (3σ) with little or no associated low ionization absorption in 3 of 10 cases. Although the number of sight lines so far sampled is small, it appears that the possibility of detecting additional C IV-HVCs through absorption line studies of this type along other sight lines is comparable to the chance of finding high velocity H I 21 cm emission along a sight line (4 of 10 cases). Further detections of C IV and/or low ionization species at high velocities along other sight lines would allow better determinations of the relationships of the C IV-HVCs and H I-HVCs. In principle, this information could be used to set a limit on the relative fraction of HVCs subject to ionization conditions like those toward Mrk 509 and PKS 2155-304. Together with the known C IV-HVCs, non-detections of C IV in the H I-HVCs toward NGC 3783 and Mrk 205 show that ionization conditions and/or gas densities vary among HVCs.

9. SUMMARY

We present new GHRS intermediate resolution ($14\text{--}18\text{ km s}^{-1}$) observations of the absorption produced by high velocity gas in the directions of Mrk 509 and PKS 2155-304. Both lines of sight have high velocity gas with unusual ionization conditions. The gas in

these “C IV-HVCs” exhibits strong C IV absorption with little or no low ion (C II, Si II) absorption or H I 21 cm emission. The C IV-HVCs present unique opportunities to study the conditions within nearby intergalactic gas and the distant Milky Way halo. The present study significantly extends our previous investigation into the properties of the C IV-HVCs described in Paper I.

The C IV-HVCs have ionization properties that are very different from those of gases in the Galactic disk and low halo. The ionic ratios are most consistent with photoionization by the relatively hard extragalactic background radiation, though contributions by hot stellar sources or collisional ionization within a hot plasma cannot be ruled out. The gas densities and cloud sizes are not well-determined due to uncertainties in the intensity of the extragalactic ultraviolet background and shape of the ionizing spectrum, but several general statements about the cloud properties can be made. If the gas is photoionized by extragalactic background radiation or a combination of ultraviolet starlight and the extragalactic background, the clouds must be low density ($n_H \sim 10^{-4} \text{ cm}^{-3}$), large (greater than several kiloparsecs), and mostly ionized ($n_{HI}/n_H \sim 10^{-3}$) regions located well beyond the neutral gas layer of the Galaxy. If the clouds are intergalactic in nature, their metallicities could be $[Z/H] \sim -1$ or lower, but higher metallicities are favored if the clouds are located in the distant Galactic halo since the cloud sizes scale inversely with metallicity.

Although we did not detect high velocity H I emission at the positions of Mrk 509 or PKS 2155-304, weak H I emissions were detected within 2° of both sight lines at velocities similar to those of the C IV-HVCs. The proximity of the C IV-HVCs and H I-HVCs in the sky indicates that the two types of high velocity gas may be related. The simplest relationship would be one in which the C IV-HVCs trace the extended, ionized low density regions of the H I-HVCs. There is no clear association of the H I or C IV-HVCs detected in our searches with large HVC complexes on the sky, though the HVCs may belong to a

group of high negative velocity H I clouds known to exist in the direction of the Galactic center.

There are several lines of evidence suggesting that the C IV-HVCs are at large distances from the Galactic plane and could possibly be intergalactic clouds in the Local Group: 1) The ionic line ratios in the C IV-HVCs do not resemble those of clouds located within the Galactic disk or low ($|z| < 5$ kpc) Galactic halo. Rather, the ionization properties of the clouds are more consistent with photoionization by extragalactic background radiation, which can only dominate the radiation field at large distances from the Galactic plane. The ionization properties of the C IV-HVCs are also similar to those of low N(H I) metal line systems seen in QSO spectra, which are known to trace intergalactic gas. 2) The inferred thermal pressures in the C IV-HVCs ($P/k \sim 2 \text{ cm}^{-3} \text{ K}$) are about three orders of magnitude lower than the thermal pressures found in the general interstellar medium in the Galactic disk or low Galactic halo. 3) A large distance (30–200 kpc) is implied if the H I-HVCs near the C IV-HVCs are in rough thermal pressure equilibrium with the C IV-HVCs. 4) There is an independent suggestion by Blitz *et al.* (1998) that the H I-HVCs in this region of the sky have a kinematical signature consistent with a location in the Local Group.

We have provided a summary of the HVCs detected in absorption at intermediate resolution with the GHRS and the IUE satellite. Ignoring the sight lines to the LMC and SMC, we find that C IV-HVCs are detected along 3 of 10 extragalactic sight lines down to a level of $\log N(\text{C IV}) \approx 13.3$ (3σ). The limited amount of data available indicates that the C IV-HVCs and H I-HVCs may have roughly similar sky covering factors.

Several measurements could be made to further reveal the nature of the C IV-HVCs. Further ultraviolet observations of the PKS 2155-304 sight line with the HST would allow stronger constraints to be placed on the ionization conditions in the C IV-HVCs along this sight line. Observations of O VI absorption with FUSE will determine whether collisional

ionization is a viable mechanism for producing some of the C IV within these clouds. Identification and investigation of additional C IV-HVCs would help constrain the typical kinematical properties and covering factors of the clouds, which could then be compared to higher redshift absorption systems.

Finally, deep H α imaging of the clouds would help to reveal the angular extents of the clouds and the spatial relationships between the H I and C IV-HVCs. By mapping out the H α emission in detail, it may be possible to set additional constraints on the distances and ionization properties of the clouds (Ferrara & Field 1994; Bland-Hawthorn *et al.* 1995; Bland-Hawthorn 1997; Tufte *et al.* 1998). For example, it may be possible to determine if collisional ionization due to ram pressure heating of the clouds as they move through a hot Galactic corona is an important contributor to the overall column densities of the ions observed in this study (particularly Si IV, C IV, and N V). We encourage those groups now performing sensitive H α emission measurements to observe the Mrk 509 and PKS 2155-304 regions of the sky.

We appreciate helpful comments about HVCs and the manuscript provided by Robert Benjamin and Bart Wakker. We thank Gary Ferland for providing a copy of the CLOUDY software and Francesco Haardt and Piero Madau for electronic versions of their ionizing spectra. KRS acknowledges support from NASA Long Term Space Astrophysics grant NAG5-3485 and from grant GO-06412.01-95A from the Space Telescope Science Institute, which is operated by AURA under NASA contract NAS5-26555. EMM acknowledges support from NASA through grant NAS5-32985. BDS appreciates support from NASA through grant NAG5-1852. LL recognizes support from Hubble Fellowship grant HF1062.01-94A.

REFERENCES

- Anders, E. & Grevesse, N. 1989, *Geochim. Cosmochim. Acta*, 53, 197
- Benjamin, R.A. & Danly, L. 1997, *ApJ*, 481, 764
- Benjamin, R.A. & Shapiro, P.R. 1998, *ApJS*, submitted
- Bergeron, J. & Stasinska, G. 1986, *A&A*, 169, 1
- Binney, J. & Tremaine, S. 1987, *Galactic Dynamics* (Princeton University Press: Princeton),
Ch. 2
- Bland-Hawthorn, J. 1997, *Pub. Astron. Soc. Australia*, 14, 64
- Bland-Hawthorn, J., Eckers, R.D., van Breugel, W., Koekemoer, A., & Taylor, K. 1995,
ApJ, 447, L77
- Blitz, L., Spergel, D., Teuben, P., Hartmann, D., & Burton, W.B. 1998, *ApJ*, submitted
(astro-ph/9803251)
- Bomans, D.J., de Boer, K.S., Koorneef, J., & Grebel, E.K. 1996, *A&A*, 313, 101
- Borkowski, K.J., Balbus, S.A., & Fristrom, C.C. 1990, *ApJ*, 355, 501
- Bowen, D., Blades, J.C., & Pettini, M. 1995, *ApJ*, 448, 662
- Brandt, J.C., Heap, S.R., Beaver, E.A., et al. 1994, *PASP*, 106, 890
- Bregman, J.N. 1980, *ApJ*, 236, 577
- Bregman, J.N. & Harrington, J.P. 1983, *ApJ*, 309, 833
- Chu, Y-H., Wakker, B., MacLow, M-M., Garcia-Segura, G. 1994, *AJ*, 108, 1696
- Cohen, R.J. & Mirabel, I.F. 1978, *MNRAS*, 182, 395
- de Boer, K.S., Morras, R., & Bajaja, E. 1990, *A&A*, 233, 523
- Dinshaw, N., Foltz, C.B., Impey, C.D., Weyman, R.J., & Morris, S.L. 1995, *Nature*, 373,

- Domgörgen, H. & Mathis, J.S. 1994, *ApJ*, 428, 647
- Donahue, M., Aldering, G., & Stocke, J.T. 1995, *ApJ*, 450, L45
- Dove, J.B. & Shull, J.M. 1994, *ApJ*, 430, 222
- Ebbets, D. 1992, Final Report of the Science Verification Program for the Goddard High Resolution Spectrograph for the Hubble Space Telescope, NASA/GSFC, Ch. 8
- Ferland, G.J. 1996, Hazy, a Brief Introduction to CLOUDY 90, University of Kentucky Physics Department Internal Report
- Ferrara, A. & Field, G.B. 1994, *ApJ*, 423, 665
- Fitzpatrick, E.L. & Savage, B.D. 1983, *ApJ*, 267, 93
- Giovanelli, R. 1981, *AJ*, 86, 1468
- Giroux, M.L. & Shull, J.M. 1997, *AJ*, 113, 1505
- Haardt, F. & Madau, P. 1996, *ApJ*, 461, 20
- Heap, S.R., Brandt, J.C., Randall, C.E., et al. 1995, *PASP*, 107, 871
- Hernquist, L., Katz, N., Weinberg, D.H., & Miralda-Escudé, J. 1996, *ApJ*, 457, L51
- Houck, J.C. & Bregman, J.N. 1990, *ApJ*, 352, 506
- Jenkins, E.B., Wallerstein, G., & Silk, J. 1976, *ApJS*, 32, 681
- Jenkins, E.B., Wallerstein, G., & Silk, J. 1984, *ApJ*, 278, 649
- Lin, D.N.C., Jones, B.F., & Klemola, A.R. 1995, *ApJ*, 439, 652
- Lockman, F.J. & Savage, B.D. 1995, *ApJS*, 97, 1
- Lu, L., Sargent, W.L.W., Barlow, T.A., Churchill, C.W., & Vogt, S.S. 1996, *ApJS*, 107, 475
- Lu, L., Savage, B.D., & Sembach, K.R. 1994a, *ApJ*, 426, 563
- Lu, L., Savage, B.D., & Sembach, K.R. 1994b, *ApJ*, 437, L119

- Lu, L., Savage, B.D., Sembach, K.R., Wakker, B.P., Sargent, W.L.W., & Oosterloo, T.A. 1998, *AJ*, 115, 162
- Madau, P. 1992, *ApJ*, 389, L1
- McKee, C.F. 1993, in *Back to the Galaxy*, eds. S. Holt & F. Verter, (AIP: New York), 431
- Mihalas, D. & Binney, J. 1981, *Galactic Astronomy*, 2nd ed., (San Francisco: Freeman), Ch. 6
- Miller, W.W. & Cox, D.P. 1993, *ApJ*, 417, 579
- Mirabel, I.F. 1981, *ApJ*, 247, 97
- Mirabel, I.F. 1982, *ApJ*, 256, 112
- Mirabel, I.F. & Cohen, R.J. 1979, *MNRAS*, 188, 219
- Mirabel, I.F. & Morras, R. 1984, *ApJ*, 279, 86
- Miralda-Escudé, J., Cen, R., Ostriker, J.P., & Rauch, M. 1996, *ApJ*, 471, 582
- Moore, B. & Davis, M. 1994, *MNRAS*, 270, 209
- Moore, C.E. 1970, *Ionization Potentials and Ionization Limits Derived from the Analysis of Optical Spectra*, NSRDS-NBS Rep. 34, Washington, D.C.: US Dept. of Commerce
- Morton, D.C. 1991, *ApJS*, 77, 119
- Murphy, E.M., Lockman, F.J., & Savage, B.D. 1995, *ApJ*, 447, 642
- Norman, C.A. & Ikeuchi, S. 1989, *ApJ*, 345, 372
- Oort, J.H. 1970, *A&A*, 7, 381
- Petitjean, P., Mucket, P.J., & Kates, R.E. 1995, *A&A*, 295, L9
- Pettini, M., Smith, L.J., King, D.L., and Hunstead, R.W. 1997, *ApJ*, 486, 665
- Prochaska, J.X. & Wolfe, A.M. 1996, *ApJ*, 470, 403

- Prochaska, J.X. & Wolfe, A.M. 1997a, ApJ, 474, 140
- Prochaska, J.X. & Wolfe, A.M. 1997b, ApJ, 487, 73
- Robinson R.D., Ake, T.B., Lindler, D.J. et al. 1998, PASP, 110, 68
- Savage, B.D. 1988, in QSO Absorption Lines: Probing the Universe, eds. J.C. Blades, D.A. Turnshek, & C.A. Norman (Cambridge University Press: Cambridge), 195
- Savage, B.D. & de Boer, K.S. 1981, ApJ, 243, 460
- Savage, B.D., Jenkins, E.B., Joseph, C.L., & de Boer, K.S. 1989, ApJ, 345, 395
- Savage, B.D., Lu, L., Bahcall, J.N., Bergeron, J., Bocksenberg, A., et al. 1993a, ApJ, 413, 116
- Savage B.D., Lu, L., Weymann, R.J., Morris, S.L., Gilliland, R.L. 1993b, ApJ, 404, 124
- Savage, B.D. & Sembach, K.R. 1991, ApJ, 379, 245
- Savage, B.D. & Sembach, K.R. 1996, ARA&A, 34, 279
- Savage, B.D., Sembach, K.R., & Lu, L. 1995, ApJ, 449, 145
- Savage, B.D., Sembach, K.R., & Lu, L. 1997, AJ, 113, 2158
- Sembach, K.R. 1994, ApJ, 434, 234
- Sembach, K.R. & Savage, B.D. 1992, ApJS, 83, 147
- Sembach, K.R., Savage, B.D., & Lu, L. 1995a, ApJ, 439, 672
- Sembach, K.R., Savage, B.D., Lu, L., & Murphy, E.M. 1995b, ApJ, 451, 616 (Paper I)
- Sembach, K.R., Savage, B.D., & Massa, D. 1991, ApJ, 372, 81
- Sembach, K.R., Savage, B.D., & Tripp, T.M. 1997, ApJ, 480, 216
- Shapiro, P.R. & Field, G.B. 1976, ApJ, 205, 762
- Shull, J.M. & Slavin, J.D. 1994, ApJ, 427, 784

- Slavin, J.D. & Cox, D.P. 1992, ApJ, 392, 131
- Slavin, J.D. & Cox, D.P. 1993, ApJ, 417, 187
- Soderblom, D.R., Hulbert, S.J., Leitherer, C. & Sherbert, L.E. 1994, Goddard High Resolution Spectrograph Instrument Handbook, v5 (Space Telescope Science Institute: Baltimore)
- Songaila, A., & Cowie, L.L. 1996, ApJ, 112, 335
- Spitzer, L. 1978, Physical Processes in the Interstellar Medium (Wiley: New York), Ch. 3
- Spitzer, L. 1990, ARA&A, 28, 71
- Steidel, C.C. 1990, ApJS, 74, 37
- Tufte, S.L., Reynolds, R.J., & Haffner, L.M. 1998, ApJ, 504, 773
- Wakker, B.P. et al. 1998, in preparation
- Wakker, B.P. & van Woerden, H. 1991, A&A, 250, 509
- Wakker, B.P. & van Woerden, H. 1997, ARA&A, 35, 217
- Walborn, N.R., Danks, A.C., Sembach, K.R., et al. 1998, ApJ, 501, L131
- Weymann, R. J., Morris, S. L., Gray, M. E., & Hutchings, J. B. 1997, ApJ, 483, 717
- Weiner, B.J. & Williams, T.B. 1996, AJ, 111, 1156
- Wheeler, J.C., Sneden, C., & Truran, J.W. 1989, ARA&A, 27, 279
- Wolfe, A.M., Turnshek, D.A., Smith, H.E., and Cohen, R.D. 1986, ApJS, 61, 249
- Wolfe, A.M., Fan, X-M., Tytler, D., Vogt, S.S., Keane, M.J., and Lanzetta, K.M. 1994, ApJ, 435, L101
- Wolfire, M.G., McKee, C.F., Hollenbach, D., & Tielens, A.G.G.M. 1995, ApJ, 453, 673

Zhang, Y., Anninos, P., & Norman, M.L. 1995, ApJ, 453, L57.

Fig. 1. - Full diode array spectra of Mrk 509 for the 1180–1216Å, 1301–1337Å, and 1383–1417Å wavelength regions. The interstellar lines in the spectra are identified, as are the high velocity cloud components associated with the C IV-HVCs observed by Sembach *et al.* (1995b). An error spectrum is shown below each spectrum. The core of the O I λ 1302 line is affected by geocoronal O I emission. Similar illustrations of the other HST spectra for Mrk 509 and PKS 2155-304 listed in Table 1 have been presented by Savage *et al.* (1997).

Fig. 2. - Continuum normalized interstellar lines observed toward Mrk 509. The data have velocity resolutions (FWHM) of 14–18 km s⁻¹ and typical continuum signal-to-noise ratios of ≈ 10 per resolution element. The pre-COSTAR data between 1231 and 1269Å have a narrow spread function core (FWHM ≈ 20 km s⁻¹) and broad wings ($\approx \pm 70$ km s⁻¹). The data in the 1230–1260Å region has considerably higher S/N (≈ 20 –30) due to the elevation in flux caused by the Ly α emission of the Seyfert galaxy. For some lines, additional absorption due to other species can be seen nearby; these features are identified in the figure. For N I, the zero velocity wavelengths of the three lines in the 1200Å triplet are indicated by vertical tick marks above the spectrum. Note the presence of high velocity clouds (HVCs) at velocities between -340 and -170 km s⁻¹ in the lines of Si III, Si IV, C IV, and possibly C II.

Fig. 3 - Continuum normalized interstellar lines observed toward PKS 2155-304. The data have velocity resolutions (FWHM) of 14–18 km s⁻¹ and continuum signal-to-noise ratios of ≈ 14 –20 per resolution element. The pre-COSTAR data shortward of 1259Å have a narrow spread function core (FWHM ≈ 20 km s⁻¹) and broad wings ($\approx \pm 70$ km s⁻¹). Note the high velocity clouds (HVCs) at -256 and -140 km s⁻¹ observed in the C IV lines. The lower velocity HVC is also seen in the strong Si II λ 1260 line, but the higher velocity cloud is unobservable in the Si II λ 1260 line due to blending with low velocity S II λ 1259 absorption.

Fig. 4 - Galactic coordinate map of the H I 21 cm emission pointings obtained for the general direction of PKS 2155-304 ($l = 17.7^\circ$, $b = -52.2^\circ$). Filled symbols indicate high

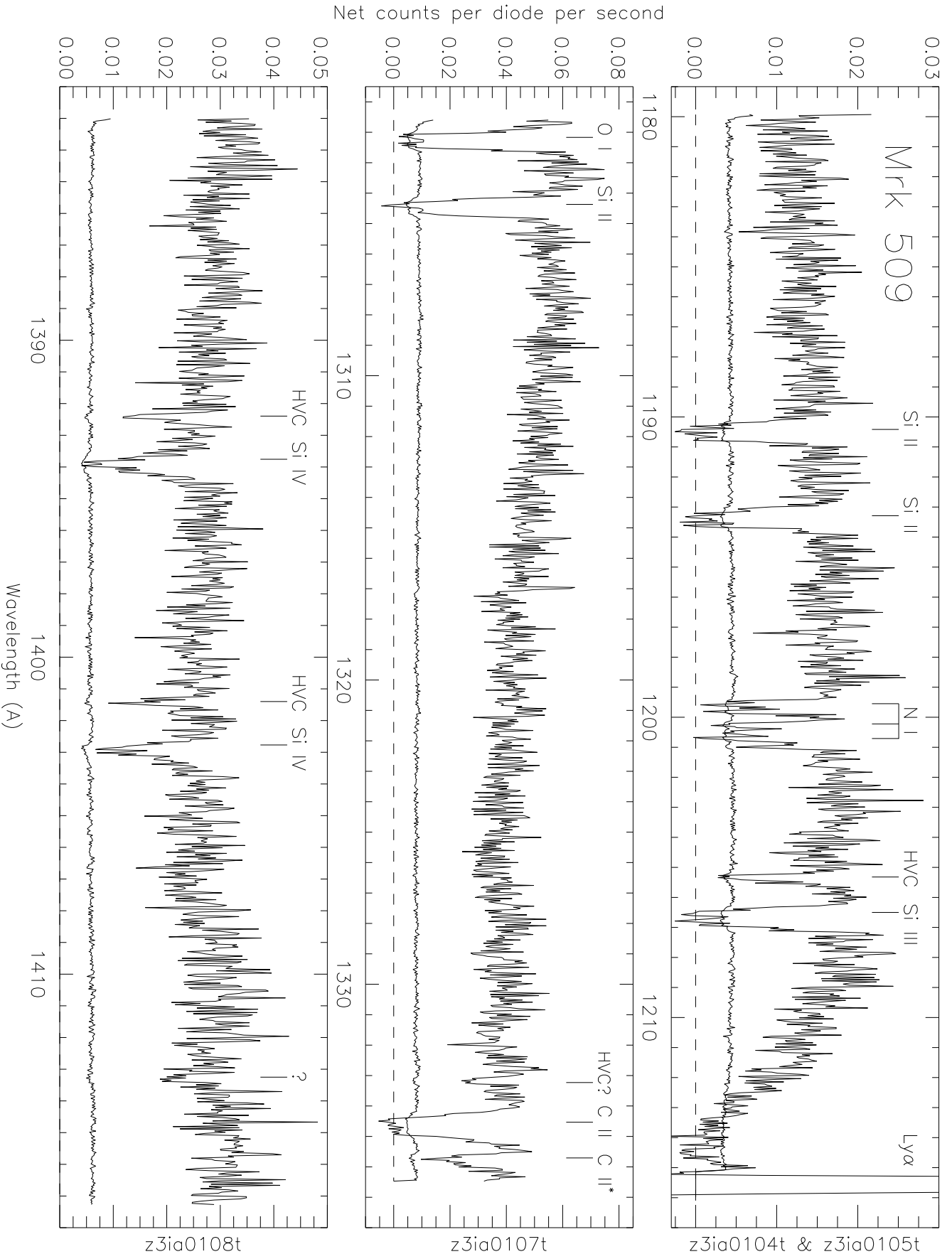
velocity H I detections; partially filled symbols indicate that the high velocity H I is partially spread out in velocity rather than concentrated as a discrete narrow feature; crosses indicate directions with no detectable high velocity H I emission. The numbers to the upper right of some symbols indicate the LSR velocities of the features detected. The spectra for pointings A–F are shown in Figure 5.

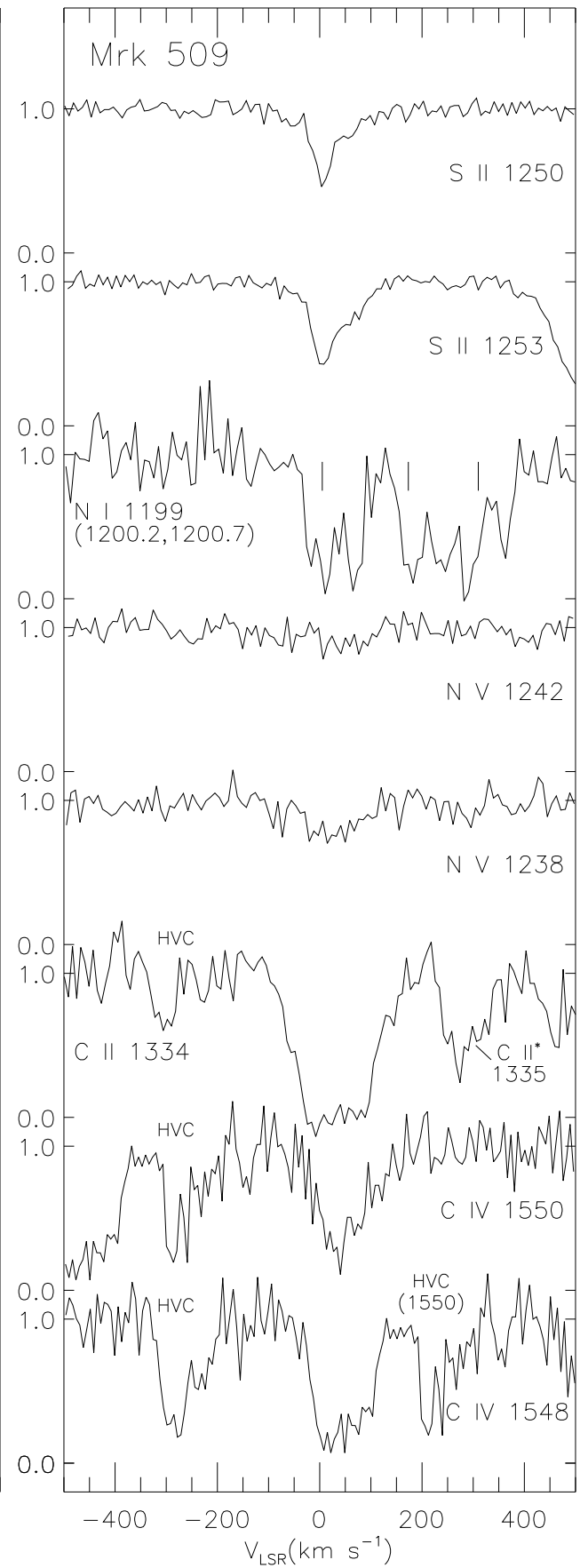
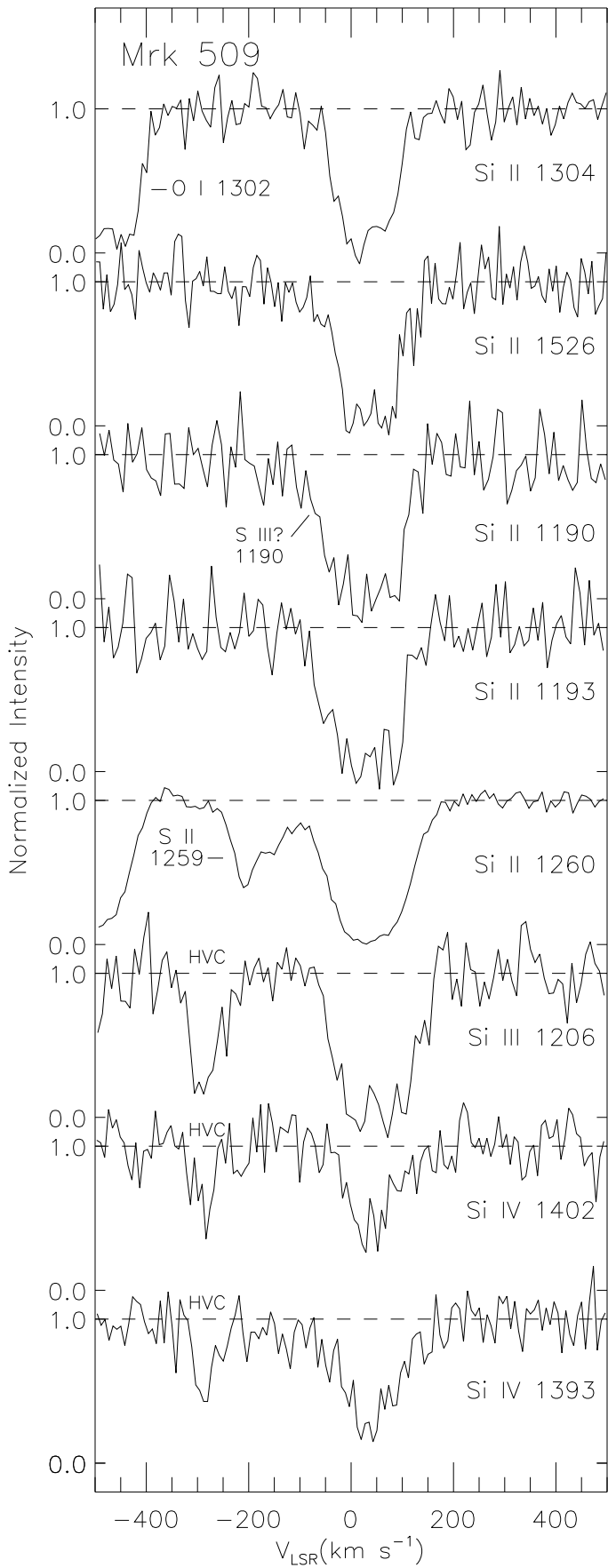
Fig. 5 - Position-switched H I 21 cm emission spectra for the PKS 2155-304 sight line and several neighboring sight lines. The brightness temperature is indicated for each spectrum on the vertical axis. Data points for velocities $|V_{\text{LSR}}| < 50 \text{ km s}^{-1}$ have been omitted since the $\pm 1.7^\circ$ position switching does not completely remove the strong signal near zero velocity. These NRAO 140-foot data have an angular resolution of $21'$ and a velocity resolution of 4 km s^{-1} after Hanning smoothing. The positions for pointings A–F are indicated in the map shown in Figure 4. A stray radiation corrected spectrum showing the emission at low velocities directly along the sight line can be found in Lockman & Savage (1995).

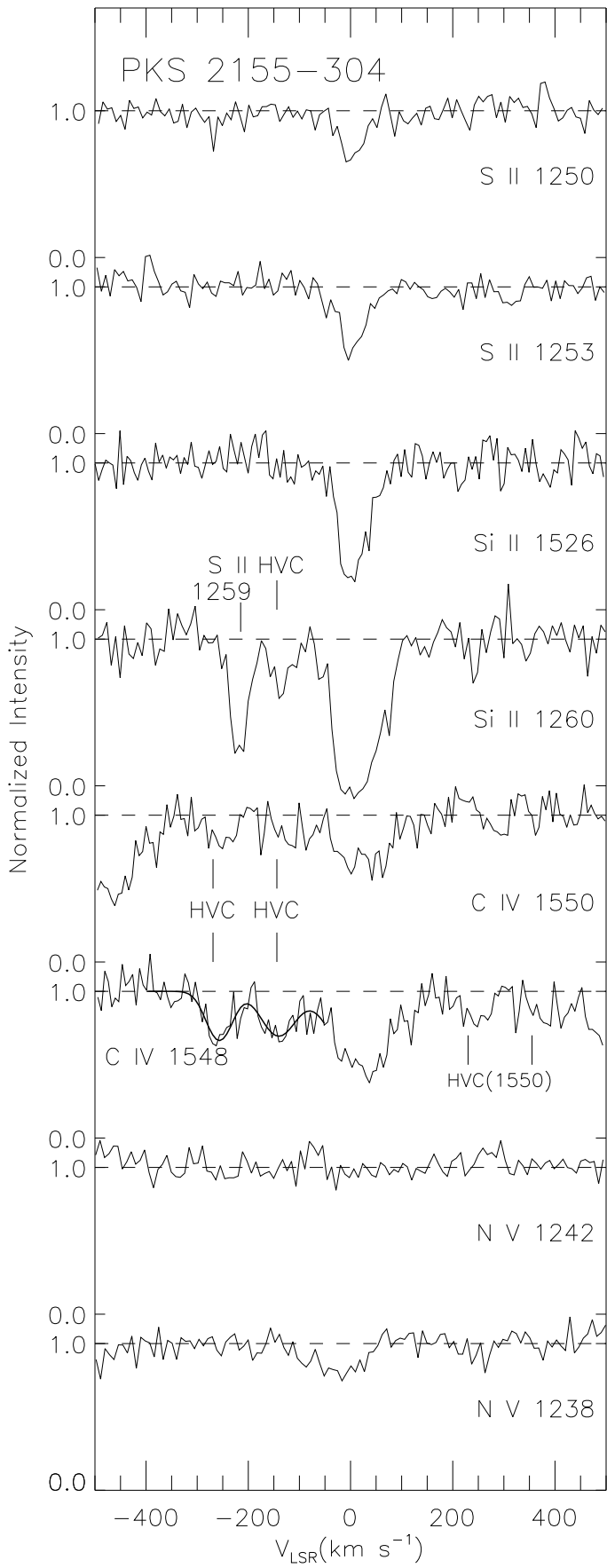
Fig. 6 - Photoionization model calculations for the ions observed toward the Mrk 509 high velocity clouds. The symbol legend contains the ion-symbol identification, and the two numbers immediately below the HVC designation indicate respectively the neutral hydrogen column density $\log N(\text{H I})$ and the gas metallicity $[\text{Z}/\text{H}]$. The mean ionizing background intensity at the Lyman limit is assumed to be $1 \times 10^{-23} \text{ erg cm}^{-2} \text{ s}^{-1} \text{ Hz}^{-1} \text{ sr}^{-1}$, though the relative column densities of the ions at a given value of Γ do not depend on the value of $J_\nu(\text{LL})$ as long as the particle density is changed accordingly. Solid lines indicate the portions of the ion curves that satisfy the observational constraints on the detections of C II, C IV, and Si IV, and the upper limits on the remaining ions. The heavy vertical line indicates the value of $\log \Gamma$ (or $\log n_H$) that allows a simultaneous fit to all of the observational constraints. The dashed line in each panel represents the predicted behavior of O VI (not observed in this study) for comparison with the other high ionization lines.

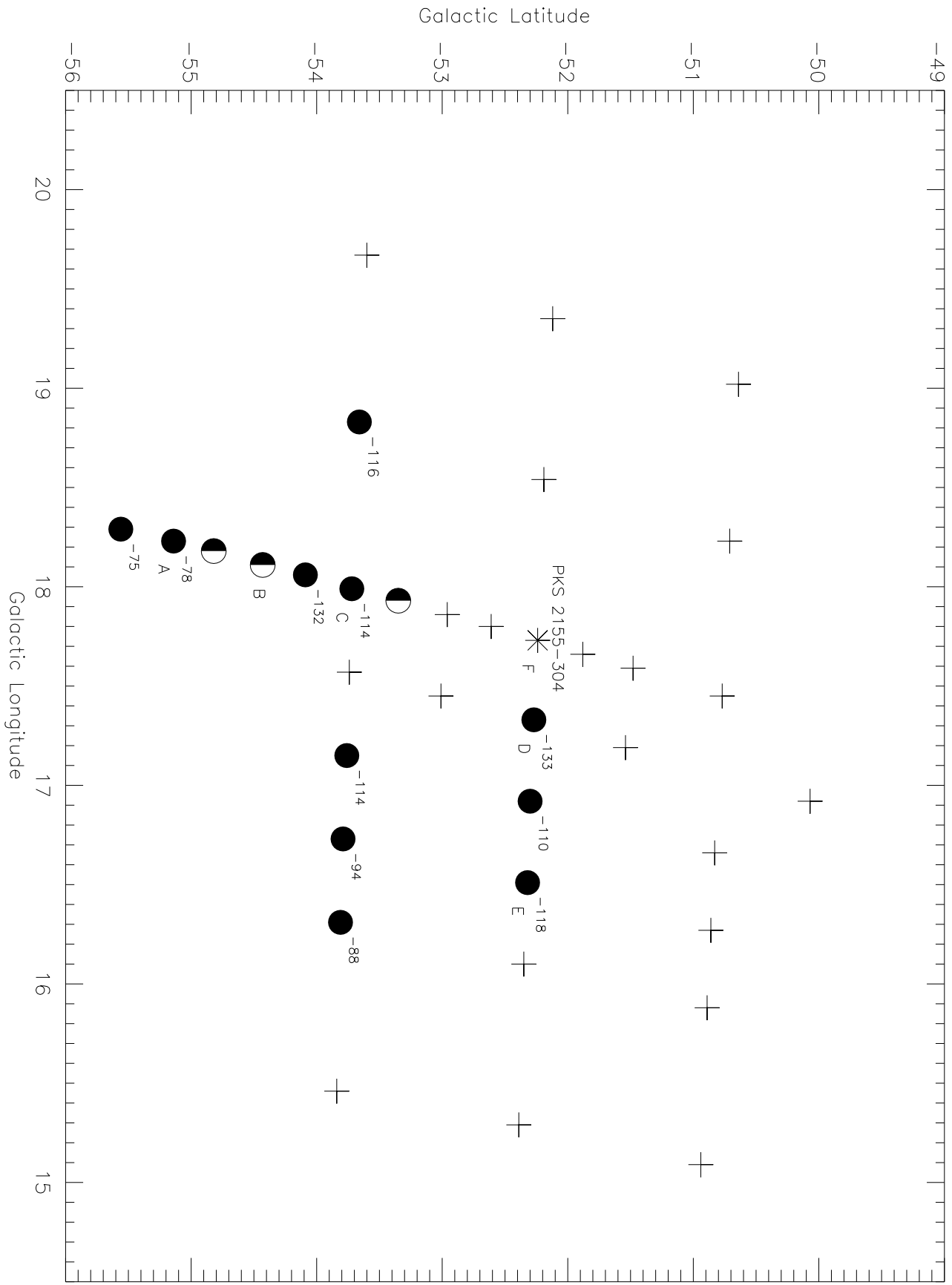
Fig. 7 - Same as Figure 6, except for the PKS 2155-304 sight line. Solid lines indicate the portions of the ion curves that satisfy the observational constraints for the C IV and Si II detections and the upper limits for the other ions.

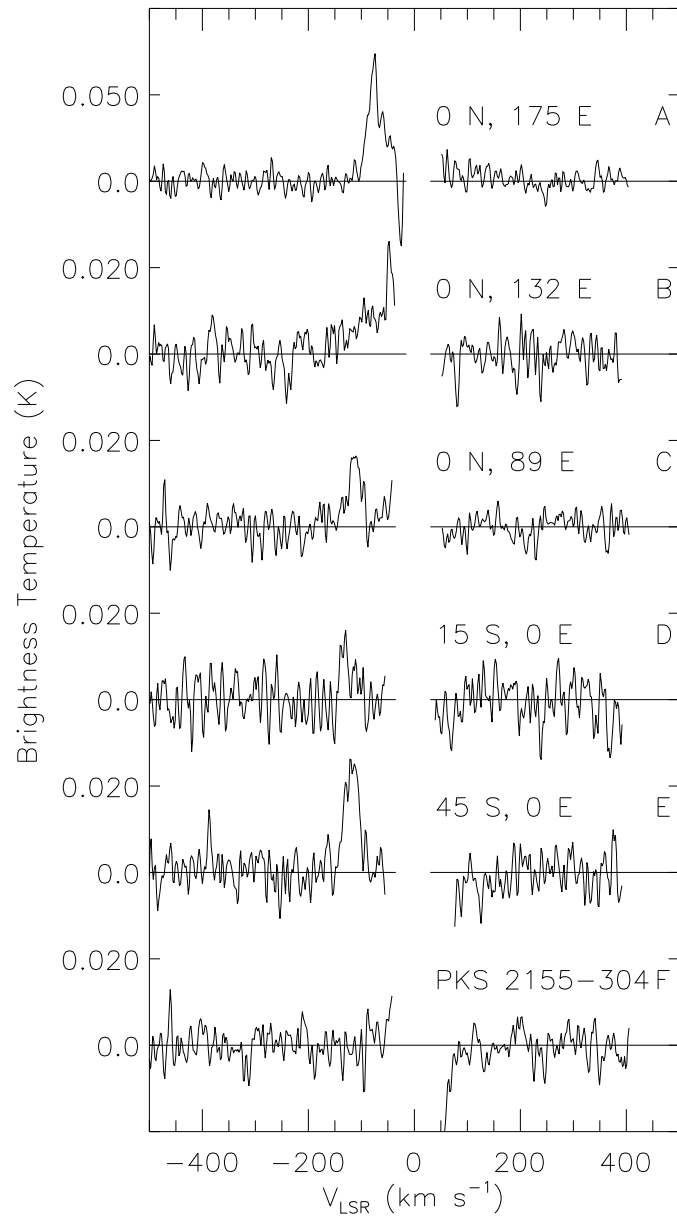
Fig. 8 - Same as Figure 6, except for a QSO power law ionizing spectrum combined with a $T_{eff} = 50,000$ K stellar spectrum. In the right hand panel, the abundance of Si relative to C has been adjusted by -0.5 dex so that a suitable fit could be found. The best fit values of Γ inferred from these panels are similar to those shown in Figure 6.

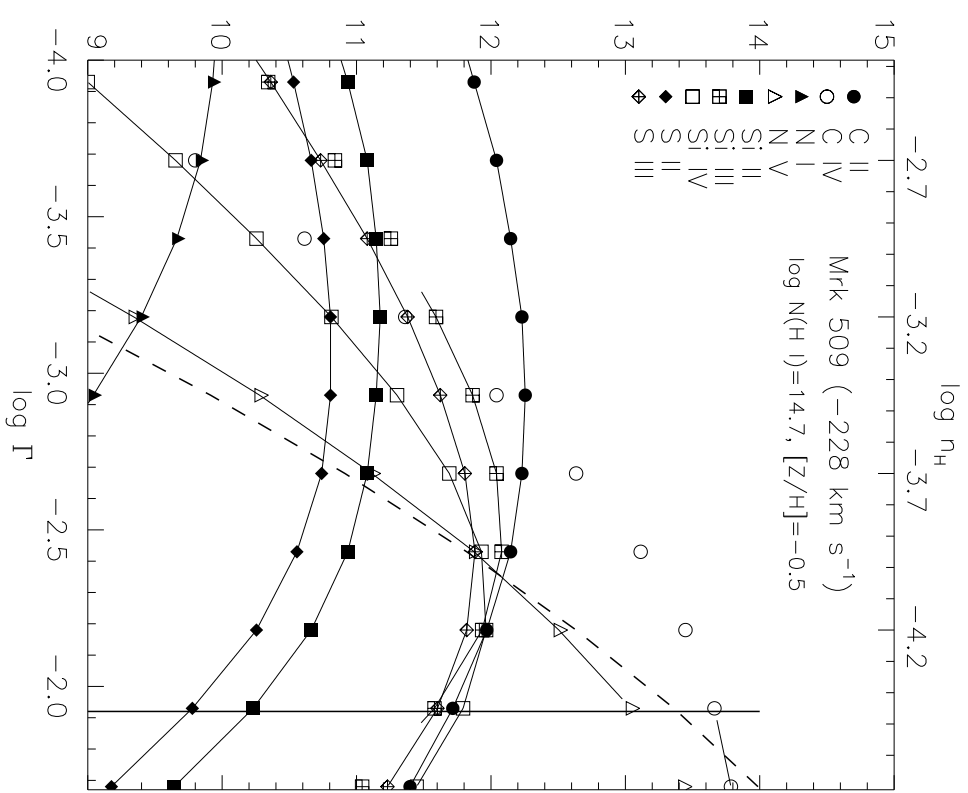
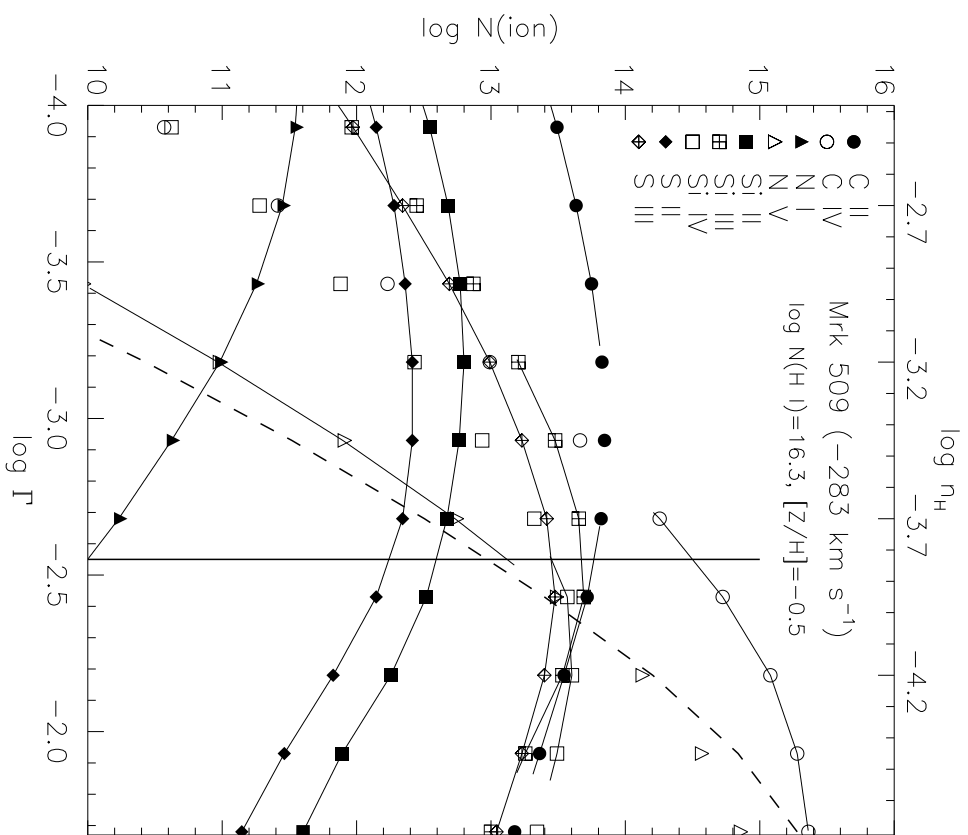


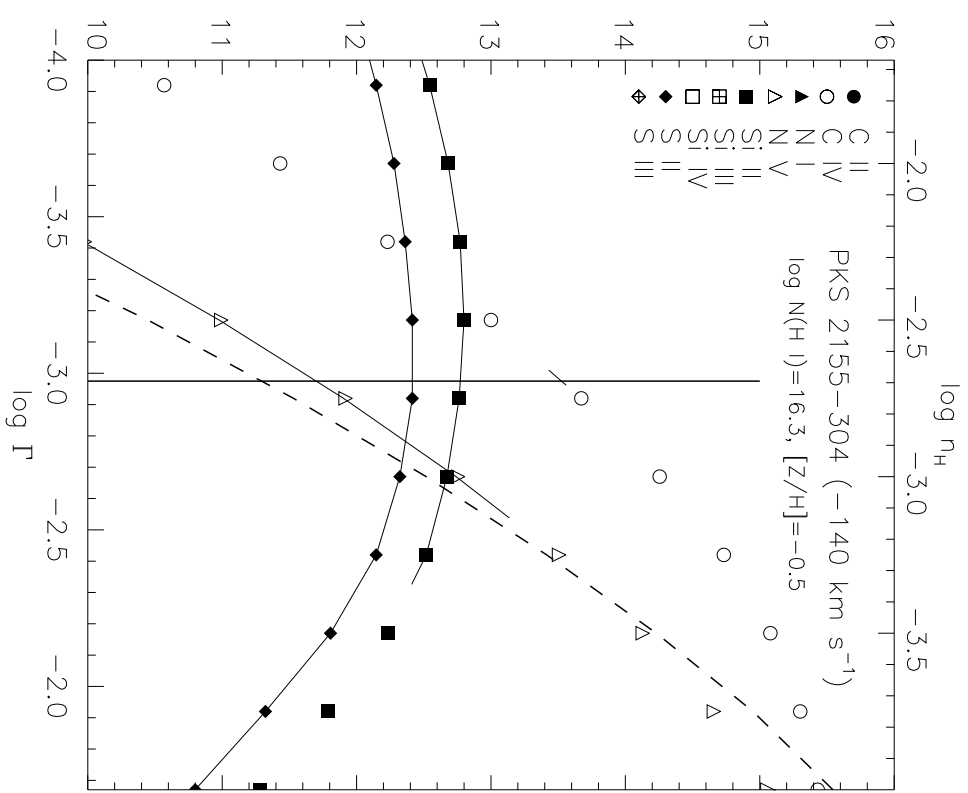
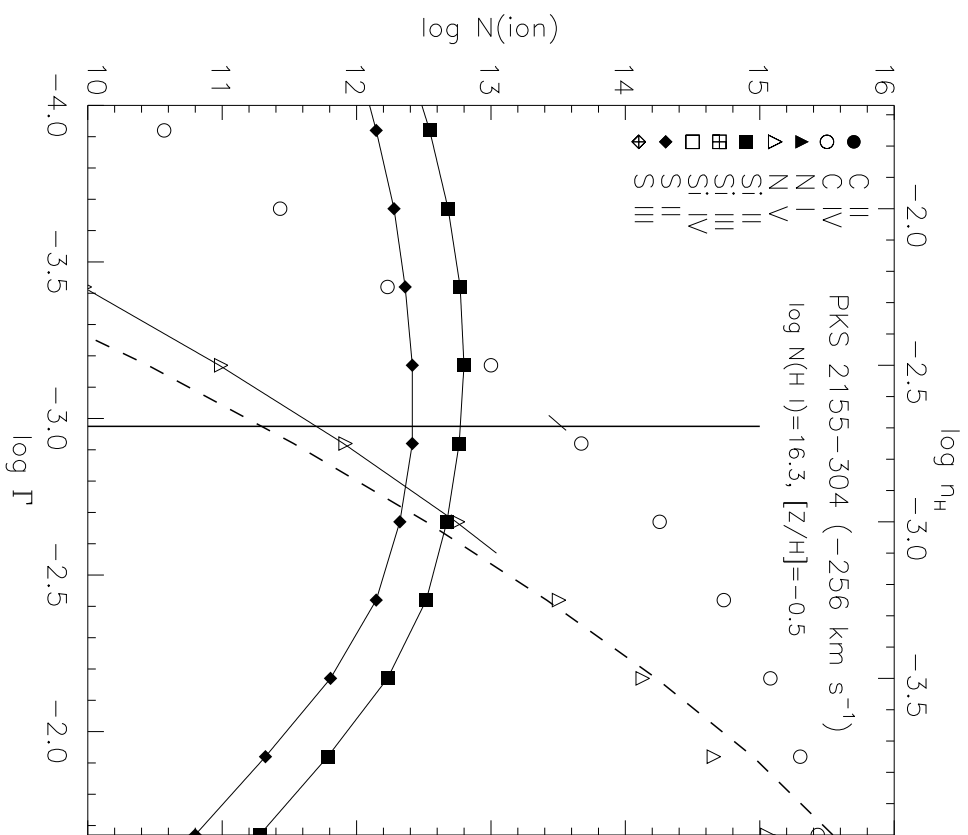












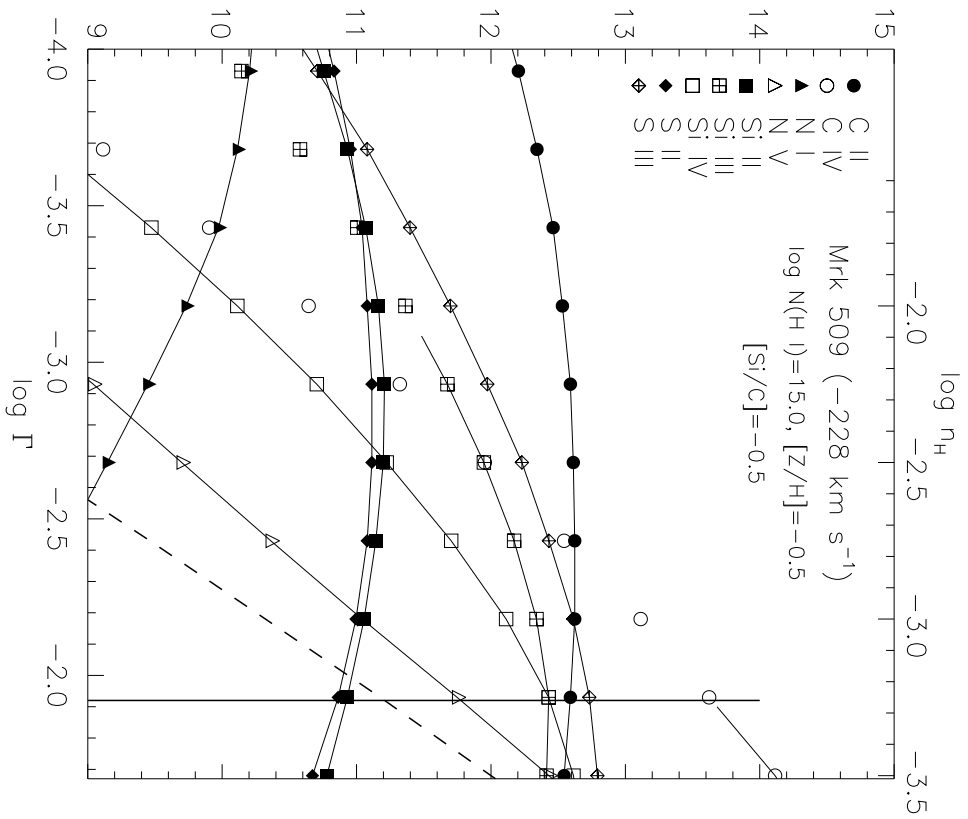
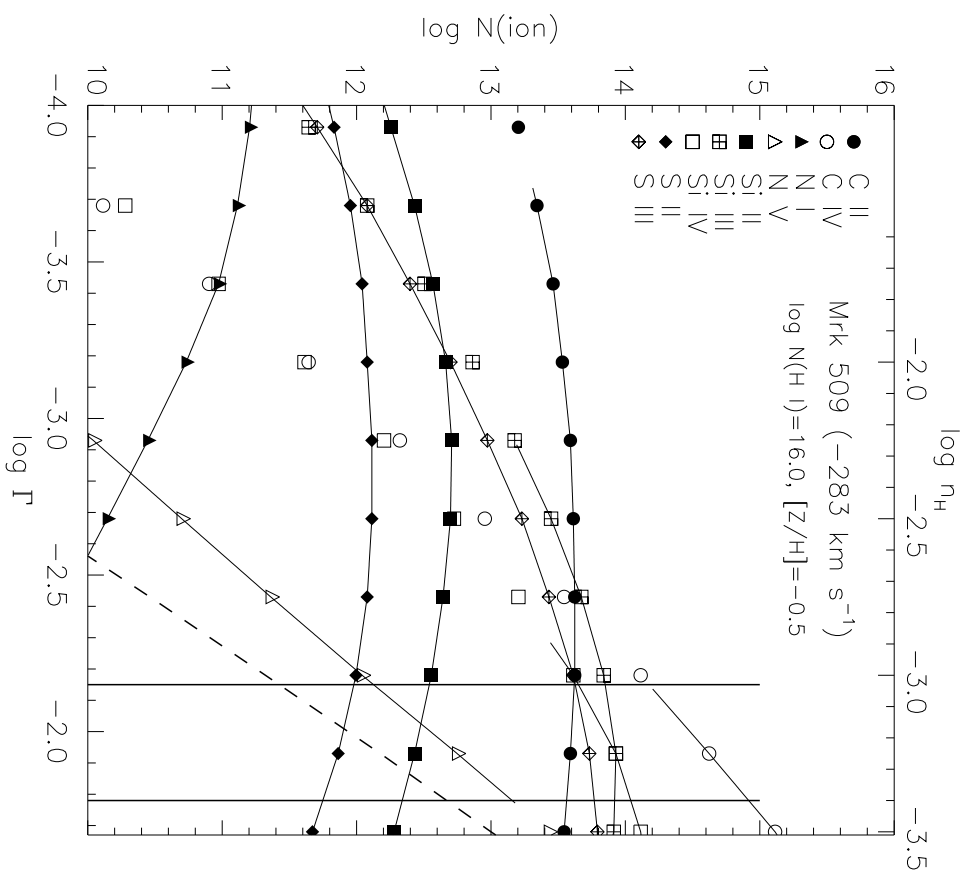


TABLE 1
GHRIS OBSERVATIONS OF MRK 509 AND PKS 2155-304

| Object | Archive ID ^a | Wavelength Coverage (Å) | Date | Stepping Pattern ^b | Exp. Time ^c (sec) | Velocity Shift ^d (km s ⁻¹) | ISM Species Detected | Original Reference ^e |
|--------------|-------------------------|-------------------------|-------|-------------------------------|------------------------------|---|-------------------------|---------------------------------|
| Mrk 509 | Z1790208M | 1231.8–1269.0 | 5/93 | 4 | 6144.0 | +10 | N v, S II, Si II | 2,3 |
| | Z2600108T | 1521.2–1557.5 | 8/94 | 4 | 7168.0 | 0 | Si II, C IV | 2,3 |
| | Z3IA0104T | 1178.8–1216.1 | 10/96 | 5 | 2867.2 | 0 | Si II, Si III | 1 |
| | Z3IA0105T | 1178.8–1216.1 | 10/96 | 5 | 2867.2 | 0 | Si II, Si III | 1 |
| | Z3IA0107T | 1300.5–1337.5 | 10/96 | 5 | 3379.2 | -10 | O I, Si II, C II, C II* | 1 |
| | Z3IA0108T | 1381.9–1418.6 | 10/96 | 5 | 4901.6 | 0 | Si IV | 1 |
| PKS 2155-304 | Z1AW0106T | 1222.7–1258.8 | 5/93 | 4 | 1574.4 | - 5 | S II, N v? | 3 |
| | Z1AW0107T | 1222.7–1258.8 | 5/93 | 4 | 1574.4 | - 5 | S II, N v? | 3 |
| | Z1AW0108M | 1222.7–1258.8 | 5/93 | 4 | 1536.0 | - 5 | S II, N v? | 3 |
| | Z3E70504T | 1257.6–1293.6 | 10/96 | 5 | 4080.0 | + 5 | S II, Si II | 1,4 |
| | Z3E70505T | 1257.6–1293.6 | 10/96 | 5 | 3400.0 | + 5 | S II, Si II | 1,4 |
| | Z2WS0107P | 1519.8–1556.1 | 10/95 | 4 | 4915.2 | 0 | Si II, C IV | 3 |
| | Z2WS0108P | 1519.8–1556.1 | 10/95 | 4 | 1024.0 | 0 | Si II, C IV | 3 |

^aAll observations were obtained in the large science aperture using grating G160M. Comb-addition and FP-SPLIT=4 were used in all cases, except for the PKS 2155-304 1222–1293Å integrations. Observations beginning with “Z1” are pre-COSTAR spectra, which have a narrow core containing ≈40% of the spread function area and broad wings containing ≈60% of the area. Observations beginning with “Z2” or “Z3” are post-COSTAR spectra with spread functions having ≈70% of the area contained within a narrow core (see text).

^bDetector substepping pattern used. STEP-PATT=4 indicates full-diode array spectra of length 1000 points with 2 samples per diode and ≈11% overhead spent on measuring interorder background levels on regions of the detector adjacent to the spectrum. STEP-PATT=5 indicates full-diode array spectra of length 2000 points with 4 samples per diode and ≈6% overhead spent on measuring interorder background levels.

^cOn-spectrum exposure time. This time does not include time spent on background measurements.

^dThe velocity shift required to put the spectra onto a common heliocentric velocity scale. All shifts are within the uncertainty (±1 diode) of the standard GHRIS wavelength calibrations.

^eOriginal references in which full-diode array spectra have appeared: 1) This paper; 2) Paper I; 3) Savage *et al.* 1997; 4) Data kindly provided by Dr. John Stocke in advance of public release into the HST archive.

TABLE 2

NRAO 21 CM LINE PROFILE RESULTS AND HI COLUMN DENSITIES NEAR THE PKS 2155-304 SIGHT LINE^a

| l ($^{\circ}$) | b ($^{\circ}$) | North ^b ($'$) | East ^b ($'$) | T_{max} ^c (mK) | FWHM (km s^{-1}) | $\langle V_{LSR} \rangle$ (km s^{-1}) | $N(\text{H I})^d$ (10^{17} cm^{-2}) |
|-----------------------|-----------------------|-------------------------------|------------------------------|--------------------------------|--------------------------------|---|--|
| 17.73 | -52.24 | 0 | 0 | <9.2 | ... | ... | <5.4 |
| 17.45 | -50.77 | 0 | -89 | <14.0 | ... | ... | <8.2 |
| 17.59 | -51.48 | 0 | -46 | <13.6 | ... | ... | <7.9 |
| 17.66 | -51.88 | 0 | -22 | <12.8 | ... | ... | <7.5 |
| 17.80 | -52.61 | 0 | +22 | <11.6 | ... | ... | <6.8 |
| 17.86 | -52.96 | 0 | +43 | <12.4 | ... | ... | <7.2 |
| 17.93 | -53.35 | 0 | +67 | <12.0 ^e | ... | ... | <7.0 |
| 17.99 | -53.72 | 0 | +89 | 15.7 \pm 1.0 | 23.0 \pm 1.9 | -113.9 \pm 0.7 | 7.0 \pm 0.7 |
| 18.06 | -54.09 | 0 | +111 | 9.0 \pm 1.1 ^f | 54 \pm 13 ^f | -132.4 \pm 3.7 | <9.4 ^f |
| 18.11 | -54.43 | 0 | +132 | <12.1 ^e | ... | ... | <7.2 |
| 18.18 | -54.82 | 0 | +155 | <12.0 ^e | ... | ... | <7.0 |
| 18.23 | -55.14 | 0 | +175 | 64.5 \pm 2.6 | 24.6 \pm 1.4 | -77.5 \pm 0.6 | 31 \pm 2 |
| 18.29 | -55.56 | 0 | +200 | 147.2 \pm 2.0 | 33.8 \pm 0.6 | -74.9 \pm 0.2 | 97 \pm 2 |
| 18.23 | -50.71 | +30 | -89 | <16.0 | ... | ... | <9.3 |
| 18.54 | -52.19 | +30 | 0 | <14.0 | ... | ... | <8.2 |
| 18.83 | -53.66 | +30 | +89 | 15.1 \pm 1.0 ^f | 20.3 \pm 1.8 | -116.6 \pm 0.7 | 6.0 \pm 0.7 ^f |
| 19.02 | -50.64 | +60 | -90 | <11.6 | ... | ... | <6.8 |
| 19.35 | -52.12 | +60 | 0 | <12.0 | ... | ... | <7.0 |
| 19.67 | -53.60 | +60 | +90 | <12.8 | ... | ... | <7.5 |
| 16.92 | -50.07 | -15 | -133 | <17.2 | ... | ... | <10 |
| 17.19 | -51.54 | -15 | -44 | <15.6 | ... | ... | <9.1 |
| 17.33 | -52.27 | -15 | 0 | 14.1 \pm 1.4 ^f | 16.1 \pm 2.1 ^f | -132.9 \pm 1.0 | <11 ^f |
| 17.45 | -53.01 | -15 | +44 | <17.6 | ... | ... | <10 |
| 17.57 | -53.74 | -15 | +89 | <20.8 | ... | ... | <12 |
| 16.66 | -50.83 | -30 | -88 | <16.8 | ... | ... | <9.8 |
| 16.92 | -52.30 | -30 | 0 | 11.4 \pm 1.3 ^f | 42.3 \pm 5.6 ^f | -110.2 \pm 2.4 | <11 ^f |
| 17.15 | -53.76 | -30 | +88 | 16.4 \pm 1.8 ^f | 46.5 \pm 6.2 ^f | -113.7 \pm 2.6 | <15 ^f |
| 16.27 | -50.86 | -45 | -88 | <16.0 | ... | ... | <9.3 |
| 16.51 | -52.32 | -45 | 0 | 25.5 \pm 1.1 | 31.8 \pm 1.6 | -117.9 \pm 0.7 | 16 \pm 1 |
| 16.73 | -53.79 | -45 | +88 | 18.6 \pm 0.8 ^f | 87.2 \pm 5.2 ^f | -94.1 \pm 2.0 | <31 ^f |
| 15.88 | -50.89 | -60 | -88 | <12.8 | ... | ... | <7.5 |
| 16.10 | -52.35 | -60 | 0 | <12.0 | ... | ... | <7.0 |
| 16.31 | -53.81 | -60 | +88 | 19.6 \pm 1.0 | 33.9 \pm 2.3 | -88.3 \pm 0.9 | 13 \pm 1 |
| 15.09 | -50.94 | -90 | -87 | <15.6 | ... | ... | <9.1 |
| 15.29 | -52.39 | -90 | 0 | <14.8 | ... | ... | <8.6 |
| 15.46 | -53.84 | -90 | +87 | <16.4 | ... | ... | <9.6 |

TABLE 2 NOTES

^a A similar table for the Mrk 509 sight line can be found in Sembach *et al.* (1995b see their Table 2).

^b Beam position relative to PKS 2155-304 in equatorial coordinates (units are arc minutes). Negative numbers indicate positions south and west of PKS 2155-304.

^c Maximum brightness temperatures and 1σ errors for Gaussian line shape fits with the central velocities and widths listed. Upper limits (4σ) on T_{max} between -400 and -100 km s^{-1} are equal to 4 times the measured RMS baseline fluctuations when no line is present. The errors associated with detections are generally smaller than those in non-detection cases since the height of the Gaussian fit to the data is constrained by ≈ 20 independent data points.

^d H I column densities and errors (1σ) derived from the NRAO 21 cm emission line measurements. Upper limits are 4σ estimates assuming $\text{FWHM} = 30 \text{ km s}^{-1}$.

^e Broad, weak emission line may extend out to -130 km s^{-1} .

^f Weak ($T_{max} < 4\sigma$) emission line for which the listed FWHM velocity width has additional uncertainties due to baseline removal. The limit on $N(\text{H I})$ is the greater of the 4σ detection limit (assuming $\text{FWHM} = 30 \text{ km s}^{-1}$) or the measured column density.

TABLE 3
EQUIVALENT WIDTHS AND COLUMN DENSITIES FOR THE MRK 509 HVCs^a

| Ion | $\lambda(\text{\AA})^b$ | f^b | [$V_{\text{LSR}} = -340$ to -250 km s^{-1}] $W_\lambda(\text{m\AA})$ | $\log N_a$ | [$V_{\text{LSR}} = -250$ to -170 km s^{-1}] $W_\lambda(\text{m\AA})$ | $\log N_a$ | Source |
|--------|-------------------------|--------|---|---------------------------|---|---------------------------|--------|
| C II | 1334.532 | 0.1278 | 70 ± 17 | $13.63 \pm_{0.13}^{0.10}$ | 22 ± 18 | < 13.49 | 1 |
| C IV | 1550.770 | 0.0952 | 186 ± 17 | 14.20 ± 0.05 | 70 ± 18 | 13.68 ± 0.10 | 2 |
| | 1548.195 | 0.1908 | 218 ± 17 | 13.96 ± 0.04 | 89 ± 17 | 13.48 ± 0.09 | 2 |
| N I | 1199.550 | 0.1328 | 17 ± 21 | < 13.58 | -20 ± 21 | < 13.39 | 1 |
| N V | 1238.821 | 0.1570 | 10 ± 11 | < 13.18 | 3 ± 9 | < 12.98 | 2 |
| Si II | 1304.370 | 0.0934 | 5 ± 15 | < 13.40 | -6 ± 13 | < 13.27 | 1 |
| | 1526.707 | 0.1155 | -5 ± 23 | < 13.29 | 11 ± 20 | < 13.33 | 2 |
| | 1190.416 | 0.2502 | 9 ± 23 | < 13.29 | 20 ± 21 | < 13.38 | 1 |
| | 1193.290 | 0.4991 | 10 ± 23 | < 13.00 | -2 ± 21 | < 12.84 | 1 |
| | 1260.422 | 1.1150 | $< 35^d$ | $< 12.65^d$ | ... | ... | 1 |
| Si III | 1206.500 | 1.6690 | 192 ± 16 | 13.19 ± 0.05 | 41 ± 20 | $12.40 \pm_{0.25}^{0.16}$ | 1 |
| Si IV | 1402.770 | 0.2553 | 93 ± 18 | $13.44 \pm_{0.09}^{0.08}$ | 17 ± 19 | < 13.15 | 1 |
| | 1393.755 | 0.5140 | 121 ± 15 | 13.26 ± 0.06 | 36 ± 15 | < 12.93 | 1 |
| S II | 1250.584 | 0.0054 | 2 ± 6 | < 14.27 | 0 ± 5 | < 14.12 | 2 |
| | 1253.811 | 0.0109 | 3 ± 5 | < 13.93 | 0 ± 5 | < 13.82 | 2 |
| S III | 1190.208 | 0.0222 | 10 ± 23 | < 14.36 | 23 ± 20 | < 14.41 | 1 |

^aEquivalent widths and apparent column densities calculated using Eq. (1) in the text. Uncertainties are 1σ measurement errors. Limits are 2σ estimates.

^bWavelengths and f -values from the data compilation prepared by Morton (1991) with updates for the Si II lines as listed by Savage & Sembach (1996).

^cSource: (1) This paper; (2) Paper I

^dContinuum placement for the Si II $\lambda 1260$ line at these velocities is subjective and depends strongly upon the properties of the nearby S II $\lambda 1259$ absorption and the derivative of the slope near the peak of the Ly α emission profile of the Seyfert galaxy. In our analysis we adopt the more conservative column density limit derived from the other Si II lines at these velocities.

TABLE 4
EQUIVALENT WIDTHS AND COLUMN DENSITIES FOR THE PKS 2155-304 HVCs^a

| Ion | $\lambda(\text{\AA})^b$ | f^b | [V _{LSR} = -330 to -190 km s ⁻¹] | [V _{LSR} = -190 to -90 km s ⁻¹] | Source | | |
|-------|-------------------------|--------|---|--|--------|--|------------|
| | | | $W_\lambda(\text{m\AA})$ | $\log N_a$ | | $W_\lambda(\text{m\AA})$ | $\log N_a$ |
| C IV | 1550.770 | 0.0952 | 60±17 | 13.52± ^{0.10} _{0.15} | 54±14 | 13.48± ^{0.10} _{0.13} | 1 |
| | 1548.195 | 0.1908 | 104±17 | 13.49± ^{0.06} _{0.08} | 114±13 | 13.52±0.05 | 1 |
| N V | 1242.804 | 0.0782 | -1±13 | <13.40 | 6±11 | <13.42 | 1 |
| | 1238.821 | 0.1570 | -1±12 | <13.05 | <29 | <13.14 | 1 |
| Si II | 1526.707 | 0.1155 | -10±18 | <13.18 | -5±14 | <13.07 | 1 |
| | 1260.422 | 1.1150 | (<50) | (<12.86) | 72±18 | 12.73± ^{0.10} _{0.13} | 2 |
| S II | 1250.584 | 0.0054 | 30±12 | <14.78 | 2±10 | <14.46 | 1 |
| | 1253.811 | 0.0109 | 2±12 | <14.20 | -10±10 | <14.12 | 1 |
| | 1259.519 | 0.0162 | 26±21 | <14.52 | -14±18 | <14.19 | 2 |

^aEquivalent widths and apparent column densities calculated using Eq. (1) in the text. Uncertainties are 1σ measurement errors. Limits are 2σ estimates. Values in parentheses are estimates based on comparison of multiple line strengths as described in text (see also note c in Table 5)

^bWavelengths and f-values from the data compilation prepared by Morton (1991) with updates for the Si II lines as listed by Savage & Sembach (1996).

^cSource: (1) This paper; (2) This paper, with reduced data courtesy of J. Stocke.

TABLE 5
SUMMARY OF ADOPTED HVC COLUMN DENSITIES^a

| Ion | Mrk 509 | | PKS 2155-304 | |
|-------------|---|---|---|---|
| | (-283 km s ⁻¹) | (-228 km s ⁻¹) | (-256 km s ⁻¹) | (-140 km s ⁻¹) |
| H I (21 cm) | <17.69 | <17.69 | <17.73 | <17.73 |
| C II | 13.63 \pm _{0.32} ^{0.18} | <13.49 | ... | ... |
| C IV | >14.20 ^b | >13.68 ^b | 13.50 \pm _{0.07} ^{0.06} | 13.50 \pm _{0.07} ^{0.06} |
| N I | <13.58 | <13.39 | ... | ... |
| N V | <13.18 | <12.98 | <13.05 | <13.14 |
| Si II | <13.00 | <12.84 | <12.86 ^c | 12.73 \pm _{0.13} ^{0.10} |
| Si III | >13.19 | 12.40 \pm _{0.92} ^{0.28} | ... | ... |
| Si IV | >13.44 ^b | <12.93 | ... | ... |
| S II | <13.93 | <13.82 | <14.20 | <14.12 |
| S III | <14.36 | <14.41 | ... | ... |

^aAdopted ultraviolet absorption line column densities derived from the values listed in Tables 3 and 4. Errors have been converted to 2σ estimates. Limits are also 2σ estimates. The H I column density limits are 4σ estimates based on the residual RMS intensity in the baselines after removal of side lobe contamination.

^bThis lower limit is based on the apparent column densities listed in Table 3. It is consistent with the limits obtained by applying a single-component Doppler-broadened curve of growth to the measured equivalent widths. The best fit value obtained from a curve of growth analysis is approximately 0.2 dex higher than the listed limit.

^cThis limit on N(Si II) is based upon the amount of high velocity Si II that could be present within the core of the S II λ 1259.5 line given the relative equivalent widths and errors of the three S II lines observed. The value listed is for a single component with Doppler width $b(\text{Si II}) > 5 \text{ km s}^{-1}$. If $b(\text{Si II}) < 5 \text{ km s}^{-1}$, N(Si II) could be larger than the listed value. If $b(\text{Si II}) \approx b(\text{C IV}) \approx 33 \text{ km s}^{-1}$, then $\log N(\text{Si II}) \leq 12.53$.

TABLE 6
 PROPERTIES OF THE C IV-HVCs DETERMINED FROM PHOTOIONIZATION MODEL RESULTS^a

| | C IV-HVC @ -283 km s ⁻¹ | | | C IV-HVC @ -228 km s ⁻¹ | | |
|--|------------------------------------|--------------|-------------|------------------------------------|--------------|-------------|
| | [Z/H] = -1.0 | [Z/H] = -0.5 | [Z/H] = 0.0 | [Z/H] = -1.0 | [Z/H] = -0.5 | [Z/H] = 0.0 |
| log N(H) (cm ⁻²) | 19.61 | 19.05 | 18.43 | 18.66 | 18.16 | 17.61 |
| log N(H I) (cm ⁻²) | 16.80 | 16.30 | 15.70 | 15.20 | 14.70 | 14.30 |
| log Γ | -2.50 | -2.55 | -2.40 | -1.90 | -1.90 | -1.90 |
| T (K) | 19,000 | 14,800 | 9,400 | 20,000 | 19,200 | 12,300 |
| D (kpc) | 108 | 28 | 8.5 | 62 | 16 | 4.0 |
| log n _H (cm ⁻³) | -3.87 | -3.82 | -3.97 | -4.48 | -4.48 | -4.48 |
| P/k (cm ⁻³ K) ^b | 5.9 | 5.1 | 2.3 | 1.5 | 1.5 | 0.94 |
| n _H /n _{HI} | 640 | 560 | 540 | 2900 | 2900 | 2000 |

^aSample CLOUDY photoionization model results for the C IV-HVCs toward Mrk 509. Two examples that satisfy the available ionic information are provided for each cloud. The input QSO-like ionizing spectrum has a Lyman limit mean intensity of $J_{\nu}(\text{LL}) = 1 \times 10^{-23} \text{ erg cm}^{-2} \text{ s}^{-1} \text{ Hz}^{-1} \text{ sr}^{-1}$ with negligible intervening opacity, and the clouds are assumed to be plane parallel slabs irradiated on both sides. A solar abundance pattern was adopted for the calculations with an overall metallicity given by [Z/H]. For models where the metallicity is super-solar and some of the Si is incorporated into dust grains, the values of n_H, n_H/n_{HI}, and D drop by factors of 5–10 and the values of P/k increase by factors of 2–5 (see §5 for details).

^bP/k is take to be 2.3n_HT. The factor of 2.3 is appropriate for a fully ionized gas containing 10% He by number.

TABLE 7
A COMPARISON OF OBSERVED IONIC RATIOS TO THEORY^a

| Ratio | Mrk 509 HVCs | | <Disk-Halo> ^b | Hot Cooling Gas ^c | Photoionized Gas ^d | |
|----------------------|--------------|------|--------------------------|------------------------------|-------------------------------|---------|
| | -283 | -228 | | | -283 | -228 |
| High/High Ion Ratios | | | | | | |
| N(C IV)/N(N V) | >10.5 | >5.0 | 4.0±2.4 | 2.2–6.8 | 18–24 | 3.9–4.9 |
| N(C IV)/N(Si IV) | (~7.2) | >5.6 | 3.8±1.9 | 3.0–4.7 | 10–11 | 49–85 |
| N(Si IV)/N(Si III) | ... | <3.4 | <1 | ~0.10 | 0.6–1.0 | 1.7–2.8 |
| High/Low Ion Ratios | | | | | | |
| N(C IV)/N(C II) | >3.7 | >1.5 | ≪1 | ~0.01 | 5.2–7.1 | ~100 |
| N(C IV)/N(Si II) | >10 | >3.5 | ≪1 | ~0.10 | 77–88 | >1000 |
| N(Si IV)/N(Si II) | >1.7 | ... | ≪1 | ~0.02 | 7.2–8.6 | 38–90 |

^aThis table provides a comparison of the observed ionic ratios for the Mrk 509 C IV-HVCs at -283 and -228 km s⁻¹ with the ratios typically observed in disk and halo gases and those predicted by theory. Values in parentheses are based upon rough approximations obtained using a single component curve of growth to estimate the column densities.

^bHigh/High ion ratios are average results from Sembach *et al.* (1997) and Sembach & Savage (1992). High/Low ion ratios are estimates made for the low velocity gas toward Mrk 509.

^cThese cooling Galactic fountain results are from Benjamin & Shapiro (1998). The model is for radiatively cooling gas with an initial temperature of 10⁶ K. The High/Low ion ratios depend upon the assumed stopping point for the cooling calculations; higher values would be obtained if the cooling flow is observed early in its evolution when much of the flow is still very hot.

^dResults for the photoionized gas models in Table 6 are listed. These photoionized gas results depend upon the parameters of the model as described in the text.

TABLE 8

AN INVENTORY OF HVC DETECTIONS AND NON-DETECTIONS ALONG EXTRAGALACTIC SIGHT LINES FOR WHICH C IV AND LOW IONIZATION ABSORPTION LINE OBSERVATIONS ARE AVAILABLE^a

| Object | l ($^{\circ}$) | b ($^{\circ}$) | HVC Identification | V_{LSR} (km s^{-1}) | Ionized Gas HVC? | Neutral Gas HVC? | H I HVC? | Ref. ^b |
|------------------------|-----------------------|-----------------------|-----------------------|--|---------------------|---------------------|-----------------|-------------------|
| PKS 2155-304 | 17.7 | -52.2 | GCN? | -140 | C IV | Si II | No ^c | 1 |
| | | | GCN? | -256 | C IV | No | No ^c | 1 |
| NGC 5548 | 32.0 | +70.5 | ... | ... | No | No | No | 3 |
| Mrk 509 | 36.0 | -29.9 | GCN? | -228 | C IV, Si III | No | No ^c | 1,2 |
| | | | GCN? | -283 | C IV, Si III, Si IV | C II | No ^c | 1,2 |
| H 1821+643 | 94.0 | +27.4 | Outer Arm | -120 | C IV | Si II, S II, Mg II | Yes | 4 |
| | | | Unknown | -213 | C IV | No | No | 4 |
| HD 5980 (SMC) | 302.1 | -45.0 | SMC | +150 | C IV, Si IV, N V | Many ions | Yes | 11 |
| HD 36402(LMC) | 277.8 | -33.0 | LMC | +270 | C IV, Si IV | Many ions | Yes | 12,13 |
| | | | Outer Galaxy? | +130 | C IV, Si IV | Many ions | Yes | 12,13 |
| SN 1987A(LMC) | 229.7 | -31.9 | LMC | +270 | C IV, Si IV | Many ions | Yes | 14 |
| | | | Outer Galaxy? | +130 | C IV, Si IV | Many ions | Yes | 14 |
| Mrk 205 | 125.5 | +41.7 | Complex C | -147 | No | Mg II | No | 5 |
| | | | 125+41-209 | -209 | No | Mg II | Yes | 5 |
| NGC 3516 | 133.2 | +42.4 | ... | ... | No | No ^d | No | 3 |
| NGC 4151 | 155.1 | +75.1 | ... | ... | No ^e | No | No | 3 |
| NGC 3783 | 287.5 | +23.0 | 287+22+240 | +240 | No | S II, Si II, Fe II | Yes | 6,7 |
| 3C 273 | 290.0 | +64.4 | ... | ... | No | No | No | 8 |
| Fairall 9 | 295.1 | -57.8 | Mag. Stream | +170 | C IV ^f | Si II | Yes | 3,9 |
| | | | Mag. Stream | +210 | No | Si II | Yes | 3,9 |
| HD 156359 ^g | 328.7 | -14.5 | Unknown | +125 | N V | Si II | No ^h | 10 |

TABLE 8 NOTES

^a This table does not include high velocity gas detections made by the GHRS in low resolution mode or the Faint Object Spectrograph (FOS) in high resolution mode. For a summary of the FOS detections, see Table 8 of Savage & Sembach (1996). One distant Galactic star with detected high velocity gas is also included (HD 156359).

^b References: 1) This paper; 2) Sembach *et al.* 1995b - Paper I; 3) Savage *et al.* 1997; 4) Savage *et al.* 1995; 5) Bowen, Blades, & Pettini 1995; 6) Lu *et al.* 1994a; 7) Lu *et al.* 1998; 8) Savage *et al.* 1993b; 9) Lu *et al.* 1994b; 10) Sembach, Savage, & Lu 1995a; 11) Fitzpatrick & Savage (1983); 12) Savage & deBoer (1981); 13) Chu *et al.* (1994) ; 14) Savage *et al.* 1989.

^c For both the Mrk 509 and PKS 2155-304 sight lines, no high velocity H I emission is observed directly along the sight line. However, H I-HVCs exist within 2° of each sight line. See text for a discussion of the relationship of these clouds with the observed HVC absorption features.

^d The non-detection of low ionization, high velocity absorption toward NGC 3516 is based upon measurements of the weak P II line near 1532Å and the C I lines near 1560Å. The C I lines are contaminated by redshifted C IV absorption associated with the Seyfert galaxy. Better estimates of the low ionization, high velocity gas will require observations of stronger low ionization lines.

^e The relatively small redshift of NGC 4151 ($z = 0.00332$) results in a substantial overlap between the Milky Way and extragalactic C IV components seen along the path to this AGN. Here we assume the C IV components seen at $V_{\text{LSR}} = -582, +146 \text{ km s}^{-1}$, and at higher velocity (Weymann *et al.* 1997) are produced in the environment of NGC 4151 rather than in the Milky Way.

^f According to Lu *et al.* (1994b) both members of the C IV doublet reveal 2σ absorption near $+170 \text{ km s}^{-1}$, the velocity of an H I-HVC toward Fairall 9. In a mean profile formed by averaging the two C IV profiles, the C IV equivalent width between 100 and 200 km s^{-1} is $95 \pm 35 \text{ mÅ}$, corresponding to a column density of $\log N(\text{C IV}) \sim 13.5$.

^g HD 156359 is a distant ($\sim 11 \text{ kpc}$) halo star that lies approximately 2.8 kpc from the Galactic plane. It is listed here for comparison with the extragalactic sight lines. High velocity absorption associated with the $+125 \text{ km s}^{-1}$ cloud has also been detected in C II, Mg II, S II, Fe II, and Si III with the IUE satellite by Sembach *et al.* (1991). Although this HVC is seen in N V with the GHRS, it is not detected in C IV or Si IV with the IUE.

^h The nearest known H I-HVC is 6° away (#364, $V_{\text{LSR}} = +115 \text{ km s}^{-1}$ in Wakker & van Woerden 1991). However, the region was mapped coarsely on a $2^\circ \times 2^\circ$ grid.